AFIT/GEP/ENP/91D-7

Silicon Carbide Thin Film Deposition by Reactive Ion-Beam Sputtering

THESIS

Larry G. Sills
Major, USAF

AFIT/GEP/ENP/91D-7

Approved for public release; distribution unlimited.

REPORT DOCUMENTATION PAGE

Form Approved
OMB No. 0704-0188

1. AGENCY USE ONLY (Leave blank)	2. REPORT DATE	3. REPORT TYPE AND DATES COVERED
	December 1991	Master's Thesis

4. TITLE AND SUBTITLE
SILICON CARBIDE THIN FILM DEPOSITION BY REACTIVE ION-BEAM SPUTTERING

5. FUNDING NUMBERS

6. AUTHOR(S)
Larry G. Sills, Major, USAF

7. PERFORMING ORGANIZATION NAME(S) AND ADDRESS(ES)
Air Force Institute of Technology, WPAFB OH 45433-6583

8. PERFORMING ORGANIZATION REPORT NUMBER
AFIT/GEP/ENP/91D-7

9. SPONSORING/MONITORING AGENCY NAME(S) AND ADDRESS(ES)

10. SPONSORING/MONITORING AGENCY REPORT NUMBER

11. SUPPLEMENTARY NOTES

12a. DISTRIBUTION/AVAILABILITY STATEMENT
Approved for public release; distribution unlimited

12b. DISTRIBUTION CODE

13. ABSTRACT *(Maximum 200 words)*

In this study, hydrogenated amorphous silicon carbide thin films were deposited by reactive ion-beam sputtering under varying conditions, to determine whether a film's optical properties can be controlled, focusing on refractive index. Using a Kaufman type ion source to sputter a pure silicon target, three distinct series of flims were grown. The first series varied the mixture of methane and argon used in the ion-beam, holding all other parameters constant. For the second series the gas mix was fixed, and only the beam energy (beam voltage) was varied. The final series also varied beam energy, but was grown with a graphite shield next to the target to reduce metal contamination sputtered from chamber surfaces. Results show the index of refraction increased monotonically with beam energy up to a beam voltage of 1300 volts. Both the second and third series of films followed this trend, but analysis of differences in atomic composition between these two series revealed opposite trends for how the silicon to carbon content ratio and refractive index were related. More precise control of the gas flow, and sputtering from only the intended (silicon) target would have reduced experimental errors.

14. SUBJECT TERMS
Silicon Carbides, Thin Films, Sputtering, Ion Beams, Vacuum Deposition, Refractive Index

15. NUMBER OF PAGES
68

16. PRICE CODE

17. SECURITY CLASSIFICATION OF REPORT	18. SECURITY CLASSIFICATION OF THIS PAGE	19. SECURITY CLASSIFICATION OF ABSTRACT	20. LIMITATION OF ABSTRACT
Unclassified	Unclassified	Unclassified	UL

GENERAL INSTRUCTIONS FOR COMPLETING SF 298

The Report Documentation Page (RDP) is used in announcing and cataloging reports. It is important that this information be consistent with the rest of the report, particularly the cover and title page. Instructions for filling in each block of the form follow. It is important to *stay within the lines* to meet *optical scanning requirements*.

Block 1 Agency Use Only *(Leave blank)*

Block 2. Report Date. Full publication date including day, month, and year, if available (e.g. 1 Jan 88). Must cite at least the year.

Block 3. Type of Report and Dates Covered. State whether report is interim, final, etc. If applicable, enter inclusive report dates (e.g. 10 Jun 87 - 30 Jun 88).

Block 4. Title and Subtitle. A title is taken from the part of the report that provides the most meaningful and complete information. When a report is prepared in more than one volume, repeat the primary title, add volume number, and include subtitle for the specific volume. On classified documents enter the title classification in parentheses.

Block 5. Funding Numbers. To include contract and grant numbers; may include program element number(s), project number(s), task number(s), and work unit number(s). Use the following labels:

C	- Contract	PR	- Project
G	- Grant	TA	- Task
PE	- Program Element	WU	- Work Unit Accession No.

Block 6. Author(s). Name(s) of person(s) responsible for writing the report, performing the research, or credited with the content of the report. If editor or compiler, this should follow the name(s).

Block 7. Performing Organization Name(s) and Address(es). Self-explanatory.

Block 8. Performing Organization Report Number. Enter the unique alphanumeric report number(s) assigned by the organization performing the report.

Block 9. Sponsoring/Monitoring Agency Name(s) and Address(es). Self-explanatory.

Block 10. Sponsoring/Monitoring Agency Report Number. *(If known)*

Block 11. Supplementary Notes. Enter information not included elsewhere such as: Prepared in cooperation with...; Trans. of...; To be published in.... When a report is revised, include a statement whether the new report supersedes or supplements the older report.

Block 12a. Distribution/Availability Statement. Denotes public availability or limitations. Cite any availability to the public. Enter additional limitations or special markings in all capitals (e.g. NOFORN, REL, ITAR).

DOD - See DoDD 5230.24, "Distribution Statements on Technical Documents."
DOE - See authorities.
NASA - See Handbook NHB 2200.2.
NTIS - Leave blank.

Block 12b. Distribution Code.

DOD - Leave blank.
DOE - Enter DOE distribution categories from the Standard Distribution for Unclassified Scientific and Technical Reports.
NASA - Leave blank.
NTIS - Leave blank.

Block 13. Abstract. Include a brief *(Maximum 200 words)* factual summary of the most significant information contained in the report.

Block 14. Subject Terms. Keywords or phrases identifying major subjects in the report.

Block 15. Number of Pages. Enter the total number of pages.

Block 16. Price Code. Enter appropriate price code *(NTIS only)*.

Blocks 17. - 19. Security Classifications. Self-explanatory. Enter U.S. Security Classification in accordance with U.S. Security Regulations (i.e., UNCLASSIFIED). If form contains classified information, stamp classification on the top and bottom of the page.

Block 20. Limitation of Abstract. This block must be completed to assign a limitation to the abstract. Enter either UL (unlimited) or SAR (same as report). An entry in this block is necessary if the abstract is to be limited. If blank, the abstract is assumed to be unlimited.

★U.S.GPO 1990-0-273-271

AFIT/GEP/ENP/91D-7

Silicon Carbide Thin Film Deposition by Reactive Ion-Beam Sputtering

THESIS

Presented to the Faculty of the School of Engineering
of the Air Force Institute of Technology
Air University
In Partial Fulfillment of the
Requirements for the Degree of
Master of Science in Engineering Physics

Larry G. Sills, B.S.
Major, USAF

December, 1991

Preface

The purpose of this study was to determine whether a silicon carbide thin film's optical properties, in particular refractive index, can be controlled by the parameters of an ion-beam used to sputter them. If such control is possible, applications of this method offer new possibilities for producing films with specially designed optical characteristics.

Films produced and analyzed for this report show that refractive index increases monotonically with ion-beam energy for a specific range of energies. The films' atomic composition changed similarly, but instabilities in the experiment and impurities in the films emphasized the need for careful control of all aspects of the sputtering process. Future experiments with better control should improve fidelity of the data, and permit attempts to grow films with continuously varying refractive index profiles.

I wish to thank my advisor, Capt Jim Targove, for allowing me the space and time to run the show pretty much as I wished. And his urgent attention to the power supply's fatal ailments is greatly appreciated. I also wish to thank the people of the Materials Laboratory here at Wright-Patterson AFB for sponsoring this work, and allowing me free reign to use whatever of their analytical equipment I chose.

None of this would have been possible if not for the support of my wife, Terri, and my children's joyful distractions. Most of all, I thank God Almighty for getting me to AFIT and seeing me through the tough times, and especially for creating such a fascinating physical universe with which to tinker.

Larry G. Sills

Table of Contents

		Page
Preface		ii
Table of Contents		iii
List of Figures		v
List of Tables		vi
Abstract		vii
I.	Introduction	1
II.	Background	4
	2.1 Overview of Ion-Beam Sputtering	4
	2.2 The Nature of Silicon Carbide Thin Films	9
III.	Experiment	14
	3.1 Experimental Apparatus	14
	3.2 Experimental Procedures	16
	3.3 Analytical Methods Used	20
IV.	Results and Discussion	23
	4.1 General Observations	23
	4.2 Optical Properties	25
	4.3 Chemical Composition	29
	4.4 Physical Characteritics	38

Page

V. Conclusions and Recommendations 39

5.1 Conclusions 39

5.2 Recommendations 39

Appendix A. Procedure Used to Set and Measure Gas Partial Pressures 42

Appendix B. Ellipsometry 44

Appendix C. Rutherford Backscatter Spectrometry (RBS) and Elastic Recoil Detection (ERD) 48

Appendix D. Deposition Parameters 51

Appendix E. Refractive Indices, Film Thicknesses, and Extinction Coefficients 53

Appendix F. Atomic Composition Data 56

Bibliography 57

Vita 60

List of Figures

Figure		Page
1.	Kaufman Type Ion-Beam Source Core	5
2.	Secondary Ion-Beam Sputtering	7
3.	Laboratory Equipment	15
4.	Details of Vacuum Chamber	22
5.	Visual Evidence of Beam Spread	25
6.	Refractive Index Change with Gas Mix: Series 1	26
7.	Refractive Index Change with Beam Voltage: Series 2	27
8.	Refractive Index Changes with Beam Voltage: Series 3	29
9.	Series 2 and 3 Transmission Spectra for Films #42 (top) and #50 (bottom). Thicknesses are about $95nm$.	30
10.	Series 2 and 3 Transmission Spectra for Films #44 (top) and #53 (bottom). Thicknesses are about $650nm$.	31
11.	Refractive Index Changes with Si/C Content Ratio: Series 2	33
12.	Refractive Index Changes with Si/H Content Ratio: Series 2	34
13.	Refractive Index Changes with H/C Content Ratio: Series 2	35
14.	Refractive Index Changes with Si/C Content Ratio: Series 2 & 3	36
15.	H/C Content Ratio Changes with Beam Voltage: Series 2 & 3	37
16.	Sample of raw and fitted ellipsometric data for film #20 at a single angle of incidence for the ellipsometer's light beam.	46
17.	Sample of raw and ellipsometric data for film #20 showing four different angles of incidence for the ellipsometer's light beam.	47
18.	Sample Copy of RBS Data Plot	50

List of Tables

Table		Page
1.	Sputtering Yield (Atoms per Ion) of Various Elements Using Noble Gas Ions at 500 eV	8
2.	Deposition Parameters: Series 1	51
3.	Deposition Parameters: Series 2	52
4.	Deposition Parameters: Series 3	52
5.	Refractive Indices and Film Thicknesses: Series 1	53
6.	Extinction Coefficients: Series 1	53
7.	Refractive Indices and Film Thicknesses: Series 2	54
8.	Extinction Coefficients: Series 2	54
9.	Refractive Indices and Film Thicknesses: Series 3	55
10.	Extinction Coefficients: Series 3	55
11.	Atomic Percentages and Mass Density: Series 2	56
12.	Atomic Percentages and Mass Density: Series 3	56

AFIT/GEP/ENP/91D-7

Abstract

The purpose of this study was to deposit hydrogenated amorphous silicon carbide (a-SiC_x:H) thin films by reactive ion-beam sputtering (RIBS) under varying conditions to determine whether the film's optical properties can be controlled, focusing on refractive index. Such control would make possible the design of films with specific refractive index profiles.

Using a Kaufman type ion source to sputter a pure silicon target, three distinct series of films were grown. The first series varied the mixture of methane and argon used in the ion-beam, holding all other parameters constant. For the second series the gas mix was set, and only the beam energy (beam voltage) was varied. The final series was grown with a graphite shield next to the target to reduce metal contamination sputtered from chamber surfaces. The gas mix was also changed in this last series.

The films contained roughly equal amounts of silicon, carbon, and hydrogen. Results show the index of refraction increased monotonically with beam energy up to a beam voltage of 1300 volts. Both the second and third series of films followed this trend, but analysis of differences in atomic composition between these two series revealed opposite trends for how the silicon to carbon content ratio and refractive index were related. Although the separate effects of carbon and hydrogen content could not be determined explicitly, increases in hydrogen content appeared to reduce the refractive index.

Future experiments with this technique should focus on complete control of the ion-beam, more precise control of the gas flow, maximizing the deposition rate, and using other reactive gases to improve ion source performance. Infrared spectra analysis should be done on films from this study to investigate chemical bonding structure.

Silicon Carbide Thin Film Deposition

by Reactive Ion-Beam Sputtering

I. Introduction

The purpose of this thesis was to determine whether reactive ion-beam sputtering (RIBS) can be used to control optical properties of hydrogenated amorphous silicon carbide (a-SiC_x:H) thin films, focusing on refractive index. This chapter introduces a-SiC_x:H as a material of current interest in applied physics, then gives an example of how precise control of the film's refractive index can produce films with important applications. A discussion of the advantages of ion-beam sputtering over other methods for growing thin films follows. Finally, the thesis chapters are briefly reviewed.

The extremes of a-SiC_x:H materials range from a semiconductor (a-Si:H) to an insulator(a-C:H). By combining Si and C in varying proportions, the optical properties can be changed to provide materials with broad applications (1, 2). Such films have good hardness, and can be designed to be transparent to wavelengths from the infrared to the visible.

Precise control of the deposition process allows for growth of thin films with *continuously* varying properties. For example, a thin film grown with a sinusoidally varying refractive index can produce a "rugate filter," which has a stop or reflection band at a specific wavelength (3, 4, 5, 6). While rugates have been fashioned using a number of methods and materials, those methods do not lend themselves well to the production of a-SiC_x:H rugates. Combining the advantages of a-SiC_x:H films with the unique properties of rugates has broad technical applications.

There are an enormous number of methods for producing thin films of all types. Even after narrowing the subject down to only ion-based methods there are still a large number of differing techniques. Ion-beam sputtering is an ion-based method that offers some unique advantages over other processes (7, 8, 9, 10):

- Deposition can be carried out at relatively low background pressure (typically 0.1 *m*torr).
- The growing film is isolated from the ion beam.
- Angle of impact of the ions on the target material, and the spot size of the beam can be controlled.
- Ion energy and current density can be controlled independently.
- Parameter control lends itself well to automated processes.

Low background pressure reduces background gas incorporation into the film, thus reducing contamination. Also, at these pressures the mean free path for gas particles is 0.5 meters or greater. This means both ions and sputtered particles avoid collisions as they travel to or from the target, thus maintaining their energies. Growing the film away from direct effects of the ion source reduces the heat loading on the substrate, while controlling the ion flux to the target permits investigations of sputter yield and deposition processes. The most important control element used in this thesis is control of the beam energy. Independent control of the ion energy makes characterization of the effects of different beam energies relatively straightforward. Lastly, modern ion-beam sources are designed to be computer controlled, and offer an attractive way to deposit films with continuously varying properties.

Nothing is perfect, however, and ion-beam sources have their drawbacks. Due to the nature of the source, the current densities are such that deposition rates of films produced by ion-beam sputtering are typically on the order of a few Å/sec at most. This requires sputter times of many hours to achieve film thicknesses of

even one micron. But advances in ion-beam sources are ongoing, and the advantages listed above make it fully competitive with other methods (7).

For this thesis, a-SiC_x:H films were grown using a single beam of argon and methane ions directed onto a pure (99.995%) silicon target. The films were grown in three series. First the ratio of methane to argon in the beam was varied. The second series fixed the gas ratio and varied the beam energy. Beam energy was again the parameter in the final series, but graphite shielding beside the target and a slightly different gas mix changed the nature of the deposition process significantly.

Before results can be presented, a more detailed look at ion-beam sputtering and the characteristics of a-SiC_x:H films is worthwhile. Chapter II presents an overview of ion-beam sputtering, with emphasis on its application to depositing thin films. Published reports on properties of films deposited by a variety of methods are reviewed. Chapter III details the experimental equipment and procedures, and explains the analytical methods used. The results of the films' optical characteristics, atomic composition, and physical characteristics are presented in chapter IV. Finally, chapter V summarizes the general and specific conclusions reached, and lists recommendations for future experiments with RIBS.

II. Background

This chapter first describes ion-beam sputtering, then provides a review of published results for thin films grown by a number of different methods.

2.1 Overview of Ion-Beam Sputtering

In the late 1950's and early 1960's broad-beam ion sources were developed for space propulsion as ion thrusters (11). Tests with these thrusters in vacuum chambers showed heavy sputtering of the chamber walls, leading naturally to experiments with these sources for sputtering applications. These are commonly called Kaufman type sources, named after Harold R. Kaufman, their developer. The special features of Kaufmann sources make them excellent devices for sputtering experiments (8):

- Ions in the beam are monoenergetic, with an energy spread of only 1-10 eV.
- Beam energy and beam current can be changed independently.
- Beam current can be varied over a wide range.
- Sources producing beam diameters as large as $30cm$ are commercially available.

For the work in this study, the first two items were the most important. Independent control of a monoenergetic beam make beam energy the pivotal parameter.

Figure 1 diagrams a typical Kaufman source like the one used for this thesis. The view shown is a cutaway along the axis of the cylindrical ion source core. The anode is an open ended cylinder allowing the cathode to intrude from one end, and the ions of the beam to escape at the other. Gas fed into the core is ionized by electrons emitted from a tungsten wire cathode (normally 0.25 mm diameter). Magnets placed around the core force the electrons through spiralling paths to the anode, enhancing ionization. The beam exits the plasma chamber through a graphite screen grid containing approximately 1 mm diameter holes in a circular pattern. An

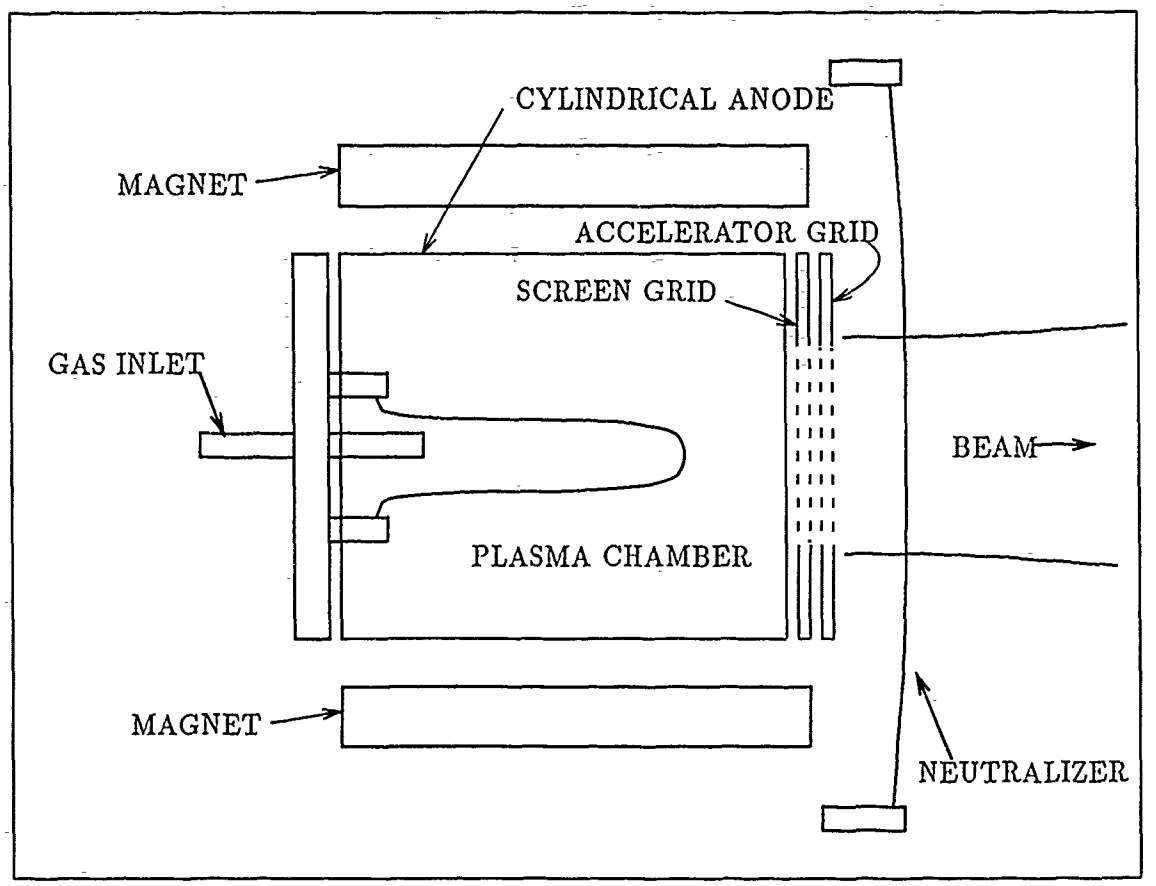

Figure 1. Kaufman Type Ion-Beam Source Core

accelerator grid, also graphite and with the same pattern of holes, is mounted about $1mm$ from the screen grid. The accelerator grid is placed at a negative potential relative to the screen grid to draw ions from the plasma, forming the beam. A hot tungsten wire called the neutralizer (also 0.25 mm diameter) is positioned across the beam and emits electrons to neutralize the plasma. This serves two purposes; an electrically neutral beam minimizes the effects of surface charges for targets made of insulating materials, and beam spread due to coulomb repulsion within the beam is reduced. It is important to realize that the neutralizing electrons do not combine with individual ions (the mean free path at normal operating pressures prevent this), but simply balance the electrical charge of the plasma. Typical beam divergence is around 10° (10:page 142).

The actual beam current is a function of plasma density and discharge voltage. The discharge voltage, the potential difference between the cathode and the anode, is typically 50 volts. For operating pressures around 0.1 $m$torr, this voltage level insures the cathode to anode current is not space-charge limited. As long as the plasma density remains constant, beam current is only a function of cathode current. Increasing the cathode current increases the number of emitted electrons, producing a higher ionization rate and ion-beam current.

Beam energy is controlled by the anode to ground potential. Beam voltage, being the anode to ground potential, is the parameter set at the ion source controller to control beam energy. A beam voltage of 1500V will produce a beam of $1{,}500eV$ ions. This is in spite of the fact that the accelerator grid has a negative potential relative to ground. This happens because, after the ions pass through the accelerator grid, they then *decelerate* back to their original energy. Thus, the net potential difference experienced by each ion in the resulting beam is just the anode to ground potential, i.e. the beam voltage.

It is important to note that the ion energies discussed here are for *singly* ionized atoms or molecules. Some of the gas could be doubly ionized, depending upon the discharge voltage and the ionization cross sections. Based on information from a study of the electron collisional ionization cross sections for CH_4(12), the CH_x fragments in the ion-beam for this study were all singly ionized. Argon, however, has an electron collisional cross section large enough for double ionization to occur(13). At the discharge voltage used ($55.0V$), the percentage of Ar^{++} ions in the ion-beam was about 5% of the total argon ion population. In experiments in which it is desirable to have *no* Ar^{++} ions in the beam, the discharge voltage must be kept below 44.0 volts. Ar^{+++} ions do not appear until the discharge voltage is greater than 88 volts.

How an experimenter uses ion-beams to grow thin films is limited only by his imagination. The specific method used for this thesis is called secondary ion-

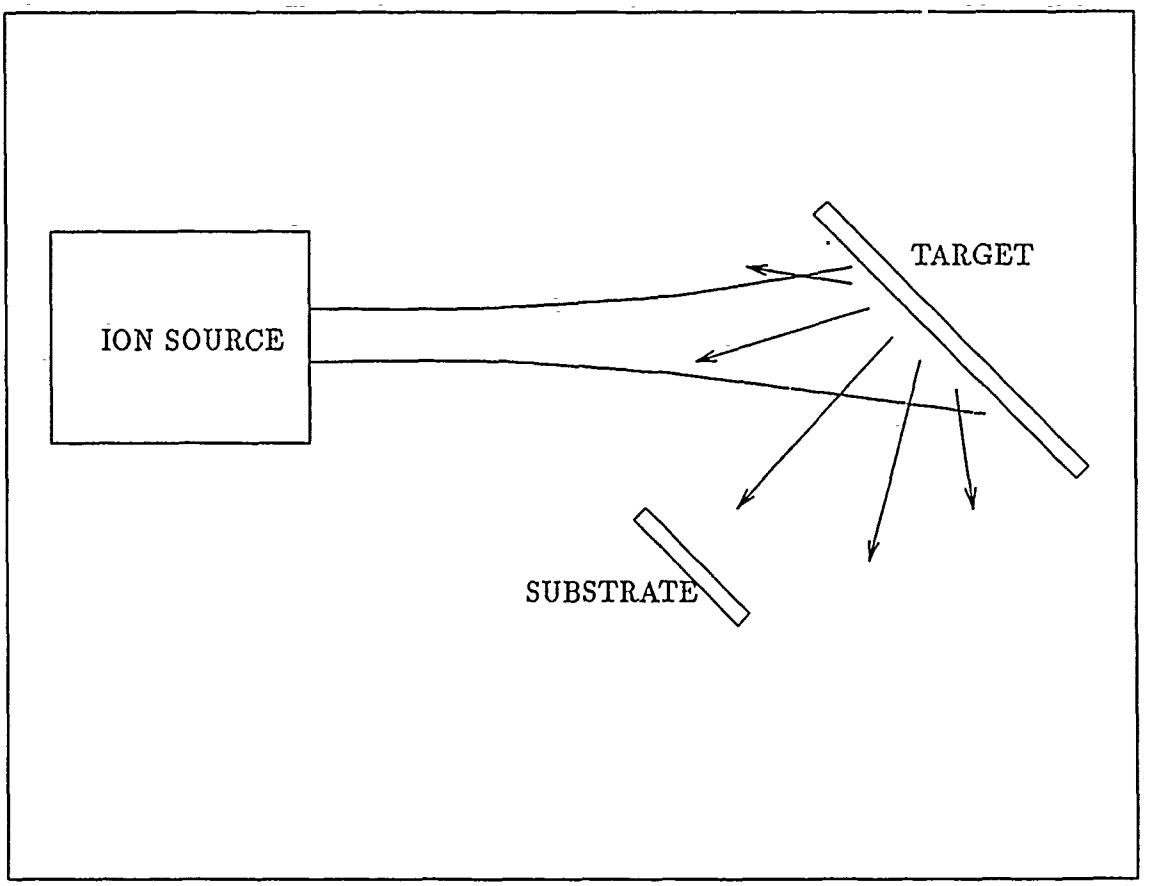

Figure 2. Secondary Ion-Beam Sputtering

beam sputtering. Figure 2 shows how this works. The ion-beam impacts the target material which is typically a single element of high purity, but compound or multiple material targets are also used (14). Atoms from the target are sputtered from the surface in all directions. For normally incident ions on most target materials at moderate beam energies (less than $10keV$), the number of atoms sputtered from a line normal to the target's surface roughly follows a cosine distribution (15:page 89). Experiments at different angles of incidence found that the exit angle for maximum emission stayed relatively constant at about 45° in a direction away from the incident ions (15:page 92). Glancing angles have a high number of reflected ions with the sputtered particles. To get the maximum sputtering rate, a 45° beam incident angle seems best (9). The substrate is positioned away from any direct effects of the beam.

Table 1. Sputtering Yield (Atoms per Ion) of Various Elements Using Noble Gas Ions at 500 eV

Noble Gas	He	Ne	Ar	Kr	Xe
element					
Be	0.24	0.42	0.51	0.48	0.35
C	0.07	-	0.12	0.13	0.17
Al	0.16	0.73	1.05	0.96	0.82
Si	0.13	0.48	0.50	0.50	0.42
Ti	0.07	0.43	0.51	0.48	0.43
Fe	0.15	0.88	1.10	1.07	1.00
Ag	0.20	1.77	3.12	3.27	3.32
Au	0.07	1.08	2.40	3.06	7.01
W	0.01	0.28	0.57	0.91	1.01
U	-	0.45	0.85	1.30	0.81

The "sputtering yield" is the number of particles sputtered for each ion impact. This yield is a complicated function of the masses of the ions and the target atoms, the beam energy, and the threshold energy required to break an atom free from the target. Theoretical predictions of the sputtering yield have been successful only for limited conditions, such as a single-element ion-beam at normal incidence to a single-element target (15:pp. 60-68). However, empirical results provide a basis for comparing sputtering yields among different target materials. Table 1 is a partial list of such yields(16:page 221). Sputtering yield also changes with ion energy. For example, at ion energies from 1000-2000eV the sputtering yield for Si increases from 0.6-0.9. This data was *not* obtained by ion-beam sputtering, but the relative yields are applicable to all sputtering methods. The author warns the reader that these numbers should be used as *relative* sputtering yields for comparison between types of ions and target materials, saying "prediction of sputtering yield in a given setup is impossible" (16:page 221-222).

The sputtered efflux from a single-element target is made up almost entirely of neutral particles with a maxwellian energy distribution (17:pages 740, 748). Mean

energy is in the range of a few eV to tens of eV. For moderate beam energies, E, the yield increases approximately proportional to $E^{\frac{1}{2}}$.

Using a pure noble gas for the ion-beam is called inert sputtering. Argon is used almost exclusively since it is available in quantity and relatively inexpensive. Reactive ion-beam sputtering (RIBS) refers to the use of one or more reactive gases in the process, which means chemical reactions are involved. Some examples of reactive gases used are oxygen, nitrogen, hydrogen, and a variety of fluorocarbons (7, 17). Since chemical reactions take place at the target and substrate, reactive sputtering is significantly different from inert sputtering. For example, a CF_x ion-beam sputtering SiO_2 at 200 eV has a sputtering yield six times greater than pure a Ar beam at the same energy (17:page 740). The complexities involved in reactive sputtering make it difficult to model, but offer almost unlimited possibilities for growing great varieties of thin films.

One of the most important issues when using ion-beams to sputter thin films is how to eliminate sources for contamination (7). Contamination is usually due to objects (other than the target) exposed to the ion-beam, e.g. surfaces of the target holder, screen and accelerator grids of the ion source, neutralizer wire. In one experiment, traces of iron ions were found in an Ar^+ beam that were eliminated only after the cathode and anode of the ion source were replaced with titanium elements (7:page 748). Whatever the application, attention must be given to minimize contamination due to impurities in the ion beam, and sputtered impurities from surfaces other than the target.

2.2 The Nature of Silicon Carbide Thin Films

For this thesis, a mixture of Ar and CH_4 (methane) was used to form the ion-beam. With such a beam, the sputtered efflux from the pure Si (silicon) target forms films with Si, C (carbon), and H (hydrogen) as the major constituents. Available literature is virtually devoid of information on RIBS using hydrocarbons. But many

articles exist on a-SiC_x:H films produced by other methods. Also, studies using RIBS with reactive gases other than hydrocarbons have interesting results applicable to non-silicon carbide films. Three of the "other" methods often used are rf sputtering, magnetron sputtering, and glow discharge (plasma) deposition. So the reader has some perspective on their differences from ion beam sputtering, a brief description of these methods is in order.

Rf sputtering is more generally known as planar diode sputtering (10). A glow discharge plasma, at a pressure around 1 *m*torr, is maintained between a cathode target material and an anode upon which the substrate is mounted. Ions colliding with the cathode target sputter neutral particles, which deposit on the substrate. Applied power is dc for metal targets and rf (13.56 MHz) for non-conducting targets. An unbiased substrate will receive particles with energies from 5-30 eV, yielding deposition rates of several Å/sec. Biasing the substrate can increase both the particle energies and deposition rates. Magnetron sputtering is similar to rf sputtering with the addition of a magnetic field parallel to the cathode surface to trap electrons near the target. This enhances ionization of the working gas, increasing the sputtering and deposition rates. A secondary effect is that sputtered particles may be ionized when passing through the relatively dense plasma trapped near the target, which can change the character of film growth. For both rf and magnetron sputtering, the deposition process can be altered simply by increasing the pressure of the plasma to as high as 70 *m*torr. The higher pressures enhance the deposition process as particles are deposited to the substrate directly from the denser plasma. This latter technique, when employed with reactive gases, is in essence plasma-enhanced chemical vapor deposition. At higher pressures than these, films can be deposited purely from the glow discharge. This plasma deposition technique uses pressures on the order of 300-600 *m*torr.

The properties of any thin film depend upon a wide range of parameters, and thus on the exact conditions during deposition (10). Although the methods described

above differ significantly from ion-beam sputtering, basic properties of films produced by other methods are informative. What follows are highlights of published results that show the optical properties and atomic composition of films grown with different techniques.

The index of refraction for a-SiC_x:H films can be related to the ratio of Si to C, and the H content of the films. Films deposited by plasma-enhanced rf sputtering in a gas mix of SiH_4 (silane) and CH_4 obtained C content ranging from 2-15 at% with a corresponding H content of 15-50 at%, depending upon the ratio of the two gases (18). Thus, the amount of hydrogen in these films was more than three times the amount of carbon, and the Si/C content ratio always exceeded 2.2. Higher C content and Si/C ratios were obtained in this study using other hydrocarbons, with similar trends. For all hydrocarbons used, the refractive index increased from 2.6 to 3.3 following Si/C ratio. In another experiment, films deposited by magnetron sputtering with Ar and CH_4 obtained C content increasing nearly linearly with CH_4 partial pressure, ranging from 20-75 at%, with the at% of H not reported (19). Ar and CH_4 were again used in rf sputtering to yield films with a C content of 30-90 at% and H content of 18-38 at% (20). In these films, the index of refraction at a wavelength of 633 *nm* varied with increasing Si/C content ratio from 2.2 to 3.2. How hydrogen incorporation affects refractive index was determined in another study (21). Films deposited by glow discharge onto heated substrates (300°C) in a CH_4-SiH_4 mixture heavily diluted with H_2 had refractive indices of 2.4-2.5. For the same Si/C ratio, films from reference (20) had indices of 3.1-3.2. This demonstrates how higher H content can significantly reduce the index of refraction.

For films deposited by glow discharge using CH_4 and SiH_4, it was found that "microvoids", spheres roughly 1 *nm* in diameter, increasingly populate the film structure as the C content increases (22). The microvoids can contain hydrogen, or just be empty "bubbles." The authors estimated the average microvoid to replace around 40 Si or C atoms that would otherwise occupy that space in the normal amorphous

lattice of the film. By their measurements, the microvoid density is on the order of 10^{20} microvoids per cm^3. Another study of bond types in glow discharge deposited a-SiC_x:H films with Si/C ratio greater than one concluded that the bonding environment of amorphous hydrogenated silicon carbide is heterogeneous due to spatially varying hydrogen and carbon bonding environments (23). However, the scale of both microvoids and bonding inhomogeneities is such that if they are uniformly distributed they should not affect refractive index.

While such inhomogeneities might be attributed to the glow discharge deposition method, there is evidence that density deficiencies can occur in sputtered films. Amorphous $SiGe_x$:H films deposited by RIBS using Ar mixed with H_2 resulted in "increased structural inhomogeneities such as voids, network strains and vacancies," and the films were "density deficient as compared to films deposited by glow discharge" (24:page 276). The higher the H_2/Ar ratio, the more density deficient and inhomogeneous the films became. Although these were not a-SiC_x:H films, the presence of significant amounts of H reacting in RIBS with a beam of Ar and CH_4 ions could cause similar deficiencies.

The chemical bonds in the film are strongly influenced by H content, as well. Films rf sputtered with a composite target of pure Si and C chips with H_2 gas introduced as a parameter, found a dramatic increase in C incorporation into the film as the flow of H_2 was increased (25). This suggests that H is preferentially bonded to C rather than Si, and that H is a necessary ingredient to get significant amount of C into the film. Another study of bond types in films prepared in a SiH_4 and C_2H_4 glow discharge found that C-H bonds out number Si-H bonds roughly 10 to 1 (26).

RIBS with a Kaufman-type ion source like the one used for this thesis produced a-Ge:H films using Ar and H for the ion beam, with pure Ge as the target (27). The authors showed that film composition changes markedly with beam energy. Specifically, the H content decreased with increasing beam energy up to a beam

voltage of 1250V, then increased for higher beam energies. The indices of refraction of these films methodically increased with beam energy, then decrease with beam voltages above 1250V. In a follow-on study, the same authors deposited a-SiGe$_x$:H films by RIBS using a composite (Si and Ge) target (28). Choosing a specific film Si/Ge content ratio (0.39), they found that the H content decreased for increasing beam energies, just as before. Again, the index of refraction rose with beam voltage, but with no trend reversal through 1500V. Both these studies suggest similar trends might be obtained for RIBS using other reactive gases, hence the subject of this thesis.

III. Experiment

As with most modern scientific experiments, equipment and experimenter have to work together in just the right way to achieve success. This chapter outlines the experimental apparatus, the procedures used to control and monitor film growth, and what analytical tools were used to make sense of it all.

3.1 Experimental Apparatus

Figure 3 shows the laboratory setup. The chamber was evacuated by a roughing pump and a molecular turbopump (Leybold 1500) in series. The ion-beam was generated by a Kaufman type ion source (Ion Tech Model 2.5-1500-125 with a MPS-5001 controller/power supply) having a 2.5 *cm* diameter beam. The deposition rate and thickness of the films was monitored using an INFICON quartz crystal. A thermocouple ionization gauge (Veeco Instruments Model RG 1000) served as the primary tool to monitor chamber pressure, with the gauge located between the chamber and the turbopump. This ionization gauge was calibrated with nitrogen gas, and all pressures reported herein are *without* applying a correction factor for CH_4 and Ar ionization differences from nitogen. Needle valves, one for Ar and one for CH_4 (both gases at least 99.999% pure), controlled the flow of gases to the ion source. The Ar and CH_4 gas lines were joined just after the valves, so the gases were mixed prior to entering the ion source. A quadrupole mass spectrometer (AMETEK Quadrupole Gas Analyzer) displayed background gas constituents, and served as a more precise tool than the ionization gauge for monitoring the Ar to CH_4 gas ratio. The ion source, Si target, and quartz crystal were water cooled using a NESLAB Instruments Coolflow 50 chiller.

Refer to figure 4 for details of the vacuum chamber. Exact location of the components within the chamber cavity was restricted by the limited space available. The Si target (99.995% pure) was placed 5.7 inches from the front face of the ion

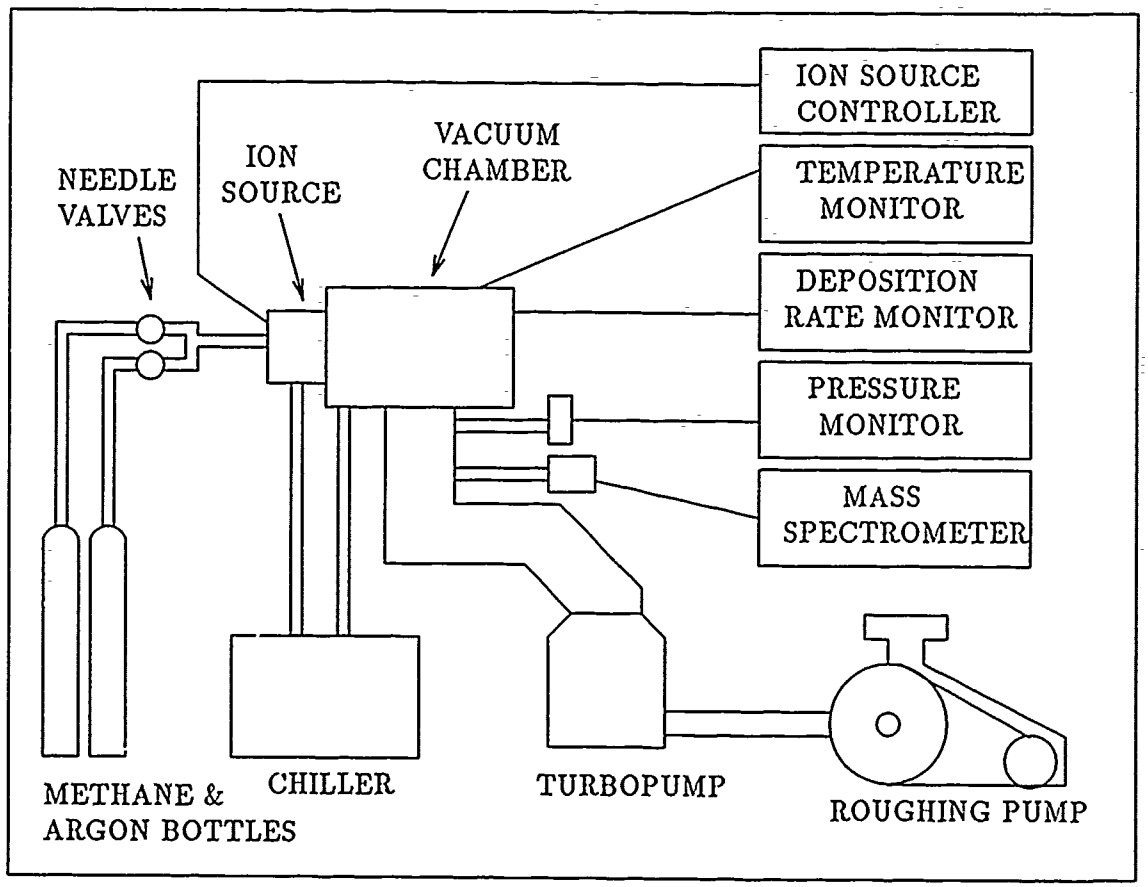

Figure 3. Laboratory Equipment

source, measured from the accelerator grid. The target angled about 10° from the vertical facing upward. The quartz crystal for the rate monitor was placed below the beam and 4 inches from the target's center. For the first two series of films, substrates were clipped to an aluminum plate and placed to the left of the quartz crystal. This placed the substrates left of center from the target. For series 3, substrates were placed over the quartz crystal mount. A moveable shutter shielded the quartz crystal and substrates from sputtered particles until time to deposit the film. The three types of substrates for the films were: crystal Si wafer slices; Be (beryllium) foil, 0.25 *mm* or 0.10 *mm* thick (99.5% pure); 1" square, $\frac{1}{16}$" thick BK-7 glass.

3.2 Experimental Procedures

Of the 38 films grown, only four failed or had to be aborted in mid-run for differing reasons. A few other runs had significant deviations during the run (gas ratio, beam current), some uncontrollable and some operator induced. Parameter control was an ongoing battle, with procedures refined and lessons learned right up to the last film sputtered.

Substrates were used "as is" from their packaging, after inspection for defects and a spray with trichlorofluoromethane to rid them of visible dust. A few early substrates were wiped with methanol and cotton swabs, but films deposited on these seemed to flake and detach in spots, owing perhaps to some residual contaminant in the methanol.

Prior to each run, the chamber was evacuated over a period of 8 hours or more. A few films were deposited with a base pressure measured slightly above 1×10^{-6} torr, but the majority began at a base pressure around 5×10^{-7} torr. At that pressure the background gas consisted of H_2O, N_2, and O_2. The base partial pressure of H_2O was always 4-5 times greater than the other two gases.

The temperature was monitored during series 2 and 3 using a Chromel-Alumel thermocouple with an Omega Model DP701 readout. The thermocouple was placed alternately near the substrate backplate, or touching the edge of the Si target.

Before sputtering began, both gas lines were purged until N_2 and O_2 partial pressures, as indicated by the mass spectrometer, were near their base levels. As long as the chamber and gas lines were at atmospheric pressure for only a few hours between runs, the gas purge took only 30-60 minutes. If the chamber was left at atmospheric pressure for a day or more, gas purge times of 2-3 hours were required.

The next step was to "pre-clean" the target by sputtering it with a pure Ar beam for at least 15 minutes, with the shutter down to protect the substrates. This insured oxides and other surface contaminants were sputtered away so as not to

contaminate the film. All pre-cleaning was done at 20-21 mA beam current and 1500V beam voltage.

After pre-cleaning, the partial pressures of CH_4 and Ar were set. This proved to be the most tedious step since the needle valves that were extremely touchy[1], and the regulator on the Ar bottle had a long settling time (30-60 min) every time the needle valve was opened. Experiences with gas flow control and the procedure adapted for it warrants further discussion.

It was only after weeks of experience with the gas valves that I discovered how barely adequate they were for precise flow control. However, with great patience, adequate control of the gas flow was attained. In fact, control of the gas pressure exceeded the precision of the ionization gauge. The ionization gauge only provided two digits and the exponent on its pressure readout. Pressure control changes of 1×10^{-6} torr increments were achievable. Changes less than 10^{-5} torr could not be displayed on the gauge's 10^{-4} torr range. To overcome this limitation, the peak heights for CH_4^+ and Ar^+ on the mass spectrometer were used to more precisely set the CH_4 and Ar partial pressures. Tiny adjustments to the gas valves were observed as changes in the relative heights of these peaks. Since the peaks were used only as a relative measurement, this technique did not depend on any calibration of the mass spectrometer. The complete procedure for setting the gas mix, developed over several weeks, can be found in appendix A.

Another important factor was how total pressure was affected by the ion source. During initial pre-sputtering, the total pressure would increase 10-20% due to out-gassing, but after 5-10 minutes settled back to the Ar pressure set prior to turning the source on. But with the CH_4 and Ar mixed, the pressure dropped 25-30% when the source was turned on, and stayed low throughout the run. Exactly how much it dropped depended on the CH_4/Ar ratio; the higher the ratio, the lower it fell. This happened because a large measure of the CH_4 ions never escaped the ion core. Car-

[1]One firm tap on the board where the valves were mounted could change the pressure ± 20%!

bon deposits were heavy on the anode, source grid, and cathode mount. To avoid confusion, the text of this report will quote only the total pressures with the ion source OFF. The tables in appendix D contain source ON and OFF total pressures for comparison.

Once the gas mix was set, the target was pre-sputtered with the CH_4:Ar beam for at least 15 minutes. This allowed the dynamics of reactive sputtering to reach a steady state. After pre-sputtering, the shutter was removed and film deposition began.

Three distinct sets, or series, of films were grown:

1. Films were grown with different ratios of CH_4/Ar, holding beam voltage, beam current, and total gas pressure constant.
2. Holding gas mix, beam current, and total gas pressure constant, films were grown at different beam voltages.
3. After installing a graphite shield to reduce metal contaminants discovered in the second series, different beam voltages and slightly reduced gas mixes[2] were used.

In the first phase, the mixture of Ar to CH_4 was varied from pure argon to an Ar to CH_4 ratio of 0.6. The total pressure of each run was set at 1.5-1.6$\times 10^{-4}$ torr. The beam current was manually controlled, and kept at 20 mA, with the beam voltage fixed at 1500V. Most films in this series were sputtered until the deposition rate monitor indicated a film thickness of 100 nm, which took a little over an hour. This works out to a deposition rate of 1.7 nm/min at the site of the quartz crystal. Actual deposition rates on substrates positioned to the left of the crystal were expected to

[2]The CH_4 to Ar partial pressure ratio was reduced (by 12% at most) to try and bring series 3 refractive indices back up near values obtained in series 2. The reason for this involved plans to attempt rugate filter growth, and the film design parameters required to do so. However, not enough time was available to pursue that goal.

be lower since they were off-axis and slightly further from the target. After six films were grown, repeat runs at a constant gas mix were made to check run-to-run uncertainty.

Using results from the first series, a gas mix with a CH_4/Ar ratio of 1.35 was chosen for the second series. Before this series began, the ion source controller failed and had to be repaired at the factory. Once back in operation, it was discovered that a stable ion-beam could be obtained only for total pressures set between 1.0-1.3$\times 10^{-4}$ torr. Thus, the second series of films was grown with a total chamber pressure 30% less than in series 2. Films were deposited to an indicated thickness (on the deposition rate monitor) of 120 nm using beam voltages from 800V to 1500V at 100V intervals. CH_4 partial pressure among runs was set from 6.2-6.9$\times 10^{-5}$ torr, and the beam current was again manually controlled at 20-21 mA. One film was grown at a beam current of 25 mA to see how the film properties would change. Another film was sputtered for 9 hours to check long term operation of the ion source.

The third and final film series modified the sputtering arrangement by placing a 0.254 mm thick graphite shield (99.9% pure) left of the target. The shield was necessary to reduce impurities sputtered from the chamber walls and plumbing, found after analysis of the second series of films. This last series varied more than one parameter in an effort to obtain film indices close to those of series 2. The gas mix ranged from a CH_4/Ar ratio of 1.15-1.45, and the beam voltage was varied from 950V to 1250V at 150V intervals. Beam current was computer controlled at 21 mA. The gas mix was changed by setting the CH_4 partial pressure (6.5-7.1$\times 10^{-5}$ torr) and increasing the partial pressure of Ar. This naturally increased the total pressure, which ranged from 1.1-1.3$\times 10^{-4}$ torr. Two films of this series were sputtered for as long as the ion source filaments would last.

Sputtering with CH_4 gradually coated the insulators in the ion core with carbon, gradually reducing their insulating resistance. The ion source had to be dis-

mantled, cleaned, and insulators replaced an average of every 2-3 runs. Cathode and neutralizer filaments lasted as many as three runs, but were usually replaced after two. Good alignment of the source and accelerator grids was very important to avoid excessive accelerator current readings.

3.3 Analytical Methods Used

Films were analyzed using four methods. A Rudolph Research S2000 Spectroscopic Ellipsometer was used with films on silicon substrates to analyze indices of refraction, extinction coefficients, and film thickness. Rutherford backscattering Spectrometry (RBS) and elastic recoil detection (ERD) (also known as forward recoil spectrometry) were performed on the Be and silicon substrates, respectively, to determine the atomic composition of the films. A Perkin-Elmer Lambda 19 spectrophotometer was used to measure %T of films on glass, and in some cases %R for films on glass or silicon. Lastly, film surface features were determined using a Park Scientific atomic force microscope. Appendices B and C contain brief discussions on, ellipsometry, RBS, and ERD.

A single run on the ellipsometer automatically measured $tan\psi$ and $cos\Delta$ over wavelengths of 300 nm to 800 nm, and separate runs were done at angles of incidence from 50° to 75°. A 70° angle of incidence yielded a good range of $tan\psi$ and $cos\Delta$ values across the spectrum. The raw ellipsometric data was analyzed on a Sun workstation using Pro-MATLAB^{TM} routines written in previous thesis work (29). To model the ellipsometric data, films were assumed to be homogeneous, with the refractive index and extinction coefficient increasing with decreasing wavelength. Recall that the complex index of refraction, N, of a material can be written

$$N = n - jk$$

where n is the real refractive index and k is the extinction coefficient. The routine used to fit the data required initial guesses for the film's n, k, and thickness. Three values for n and two or three for k at different wavelengths establish dispersion curves for each. Because the absorption spectra differed between films, the k values were chosen at wavelengths which gave the best fit. For many films, the best fit was obtained using three k values rather than two.

Knowing n and k for air and the silicon substrate, it is a straightforward but tedious matter of mathematical mechanics to calculate $tan\psi$ and $cos\Delta$ (29). The predicted curves were compared to raw ellipsometry data, and corrective guesses for n and k made manually to get a better fit. Once the fit was close, two computer routines curve fit the data to minimized error in a least squares sense. These fits were checked against each other, and against ellipsometry data taken at different angles of incidence to validate the fit. The resulting values for refractive indices across the spectrum and film thickness varied only 1-2% (see appendix E).

RBS and ERD were done through government contract with the Physics department of the University of Arizona. The numbers reported were in atoms/cm^2, which was used with film thickness to get atomic and mass density. The uncertainties in the RBS results were less than 1% for Si and C, and less than 7% for the impurities. ERD results determined H content to an uncertainty of 10%. Combining the RBS and ERD numbers yielded an uncertainty of 5% overall for atomic content.

The spectrophotometer measured the films' %T and/or %R for wavelengths from 350-900 nm. The atomic force microscope, capable of displaying features as small as individual atoms, provided a detailed look at surface features.

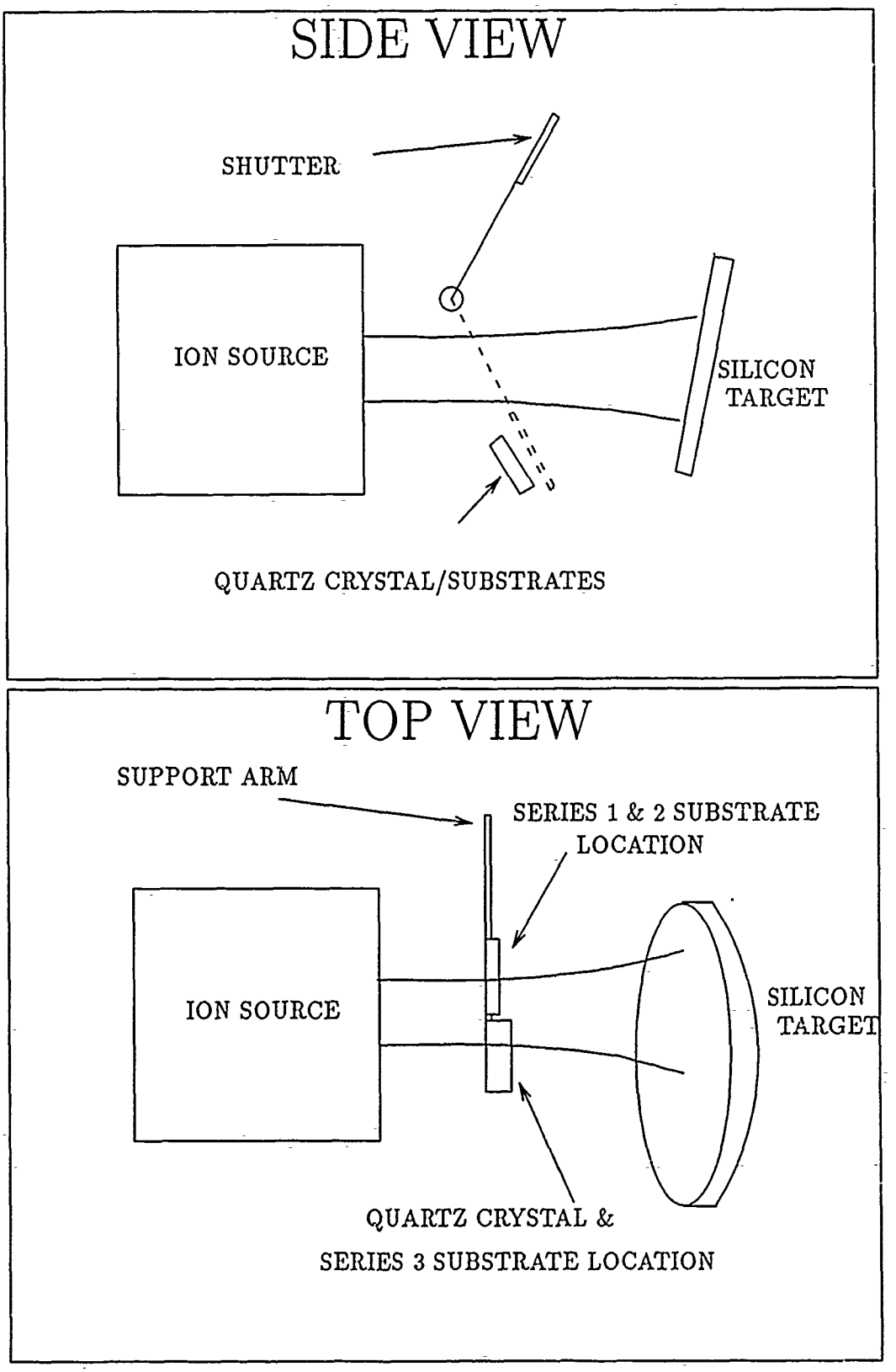

Figure 4. Details of Vacuum Chamber

IV. Results and Discussion

Large amounts of data were collected during this study, making analysis a major challenge. This chapter first reviews observations common to all films grown. The next section shows how optical properties of the three series of films relate to deposition conditions. Then, the relation between atomic composition and the films' character is presented. The last section discusses the films' adherence to the substrates and their microscopic surface features.

4.1 General Observations

Ellipsometry analysis on a silicon substrate "right out of the box" revealed a 2.2 *nm* thick oxide layer with a refractive index of 1.45. A special data fitting routine that modeled two homogeneous thin films on a known substrate was used to confirm that the presence of this oxide layer did not affect the results obtained with the single homogeneous layer routine, which was used for results presented here.

Appendix D contains a list of the deposition conditions for each successful run. Before discussing the specific results of each series of films, more general points applicable to all films need to be brought out.

A wide range of discharge currents among runs for the same beam current was due to the effects of carbon coating the insulators. The discharge current measures *total* current between the anode and all surfaces. Thus as the anode's insulators resistance decreased, the discharge current went up. Two of the four runs aborted were due to this effect. To explain, it was discovered that lightly coated insulators would show resistances in the hundreds of MΩ's at room temperature, but change to less than 1 MΩ at operating temperatures. As the insulators continued to lose effect, the discharge current heated the ion core further, further reducing insulator resistance. This "thermal runaway" eventually caused arcing damage to the anode and cathode filament failure. The ion source itself had such a long cool-down time

that attempts to divide the run into shorter sputtering periods with "cooling off" times in between met with only partial success. The only real "fix" was to replace the leaky insulators.

Temperature of the substrates was always less than 80°C, while the target temperature (measured at the target's edge - see figure 5) was as high as 185°C for the highest beam voltage (1500V). On the long term sputtering runs (8 hours or more), the outer surface of the chamber itself became very hot to the touch. Cooling for the target, quartz crystal, and ion source was adequate, and the substrate mounting plate was partially cooled simply because it was placed on the quartz crystal monitor's plumbing.

The 15 minute pre-cleaning and pre-sputtering times were confirmed to be sufficient when two films (#35 and #36) sputtered under identical conditions. One film was pre-cleaned and pre-sputtered with the standard 15 minute times and the other with 40-45 minute times for each, showing no attributable differences.

The deposition rate indicated by the quartz crystal was accurate for the crystal's location. But films grown to the left of the crystal had deposition rates about 20% less, as was expected. Deposition rate indications varied with beam voltage from 15-20 Å/min over 800-1500V. Most films were sputtered to a thickness of 70-100 *nm*. The three long term sputtering runs attained thicknesses between 500-700 *nm*.

On all three long term runs, the neutralizer filament failed after 7-8 hours. This is simply because the ion-beam sputters material from the neutralizer, wearing it thin. The cathode filament lasted from 7 to more than 10 hours. Cathode failure was accelerated whenever the thermal runaway effect occurred.

The sputtering pattern on the target was visible as a 2+ inch diameter "shiny" area centered on the left side of the target, and some faint arc shaped striations at the top right edge. Figure 5 depicts these observations, and projects the possible

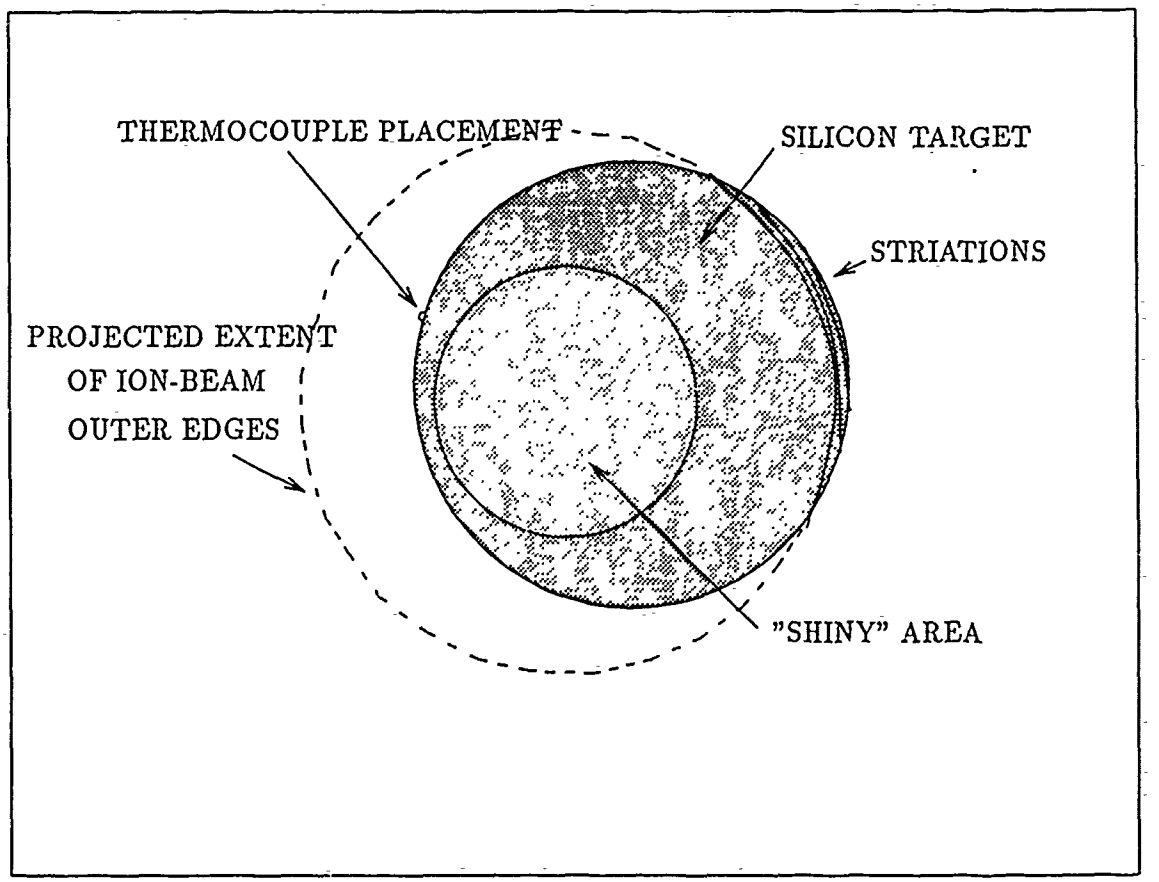

Figure 5. Visual Evidence of Beam Spread

extent of the ion beam's outermost edges. The beam spread visible to the naked eye (with the neutralizer OFF) corresponded with the shiny spot on the target. Simple trigonometry shows this spread to be slightly more than the 10° quoted in the chapter II. But if the projected size of the outermost edge of the beam is correct, the widest divergence of ions from the source is 25-30° from the beam axis.

4.2 Optical Properties

Turning now to the results from the first film series, figure 6 shows a plot of index of refraction at 800 *nm* vs CH_4/Ar partial pressure ratio. The 800*nm*wavelength index was chosen since the films' absorption was least at longer wavelengths (see appendix E for a list of refractive indices). The plot shows how increasing the CH_4/Ar

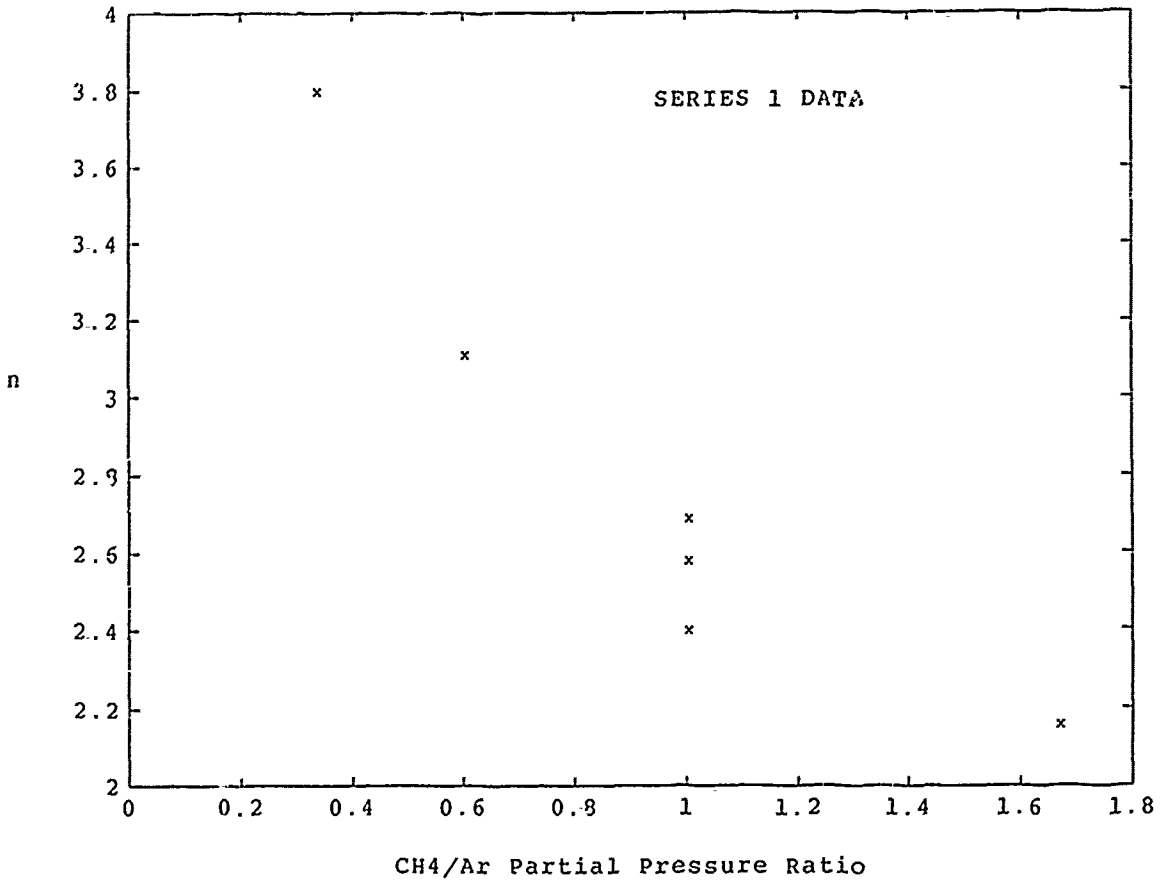

Figure 6. Refractive Index Change with Gas Mix: Series 1

gas ratio decreases the index of refraction, as expected for a decreasing Si/C content ratio in the films. The relationship cannot be linear because the index of refraction for pure a:Si at 800 *nm* is about 4.0.

Based on these results, we chose a gas mix to produce films with n(800*nm*) $\approx$ 2.6 for the second film series, for two reasons. Films with a lower refractive index could be more precisely fit to the ellipsometry data, making lower indices desirable. But this was balanced by the fact that CH_4/Ar gas ratios much higher than 1 coated the ion source insulators very quickly, limiting how long the run conditions would remain stable. However, throughout this first series the sensitivity of the gas valves and the instability in the Ar bottle regulator were not known. Thus, the uncertainty in the CH_4/Ar ratio during any run was 10-12%. And although control of the gases

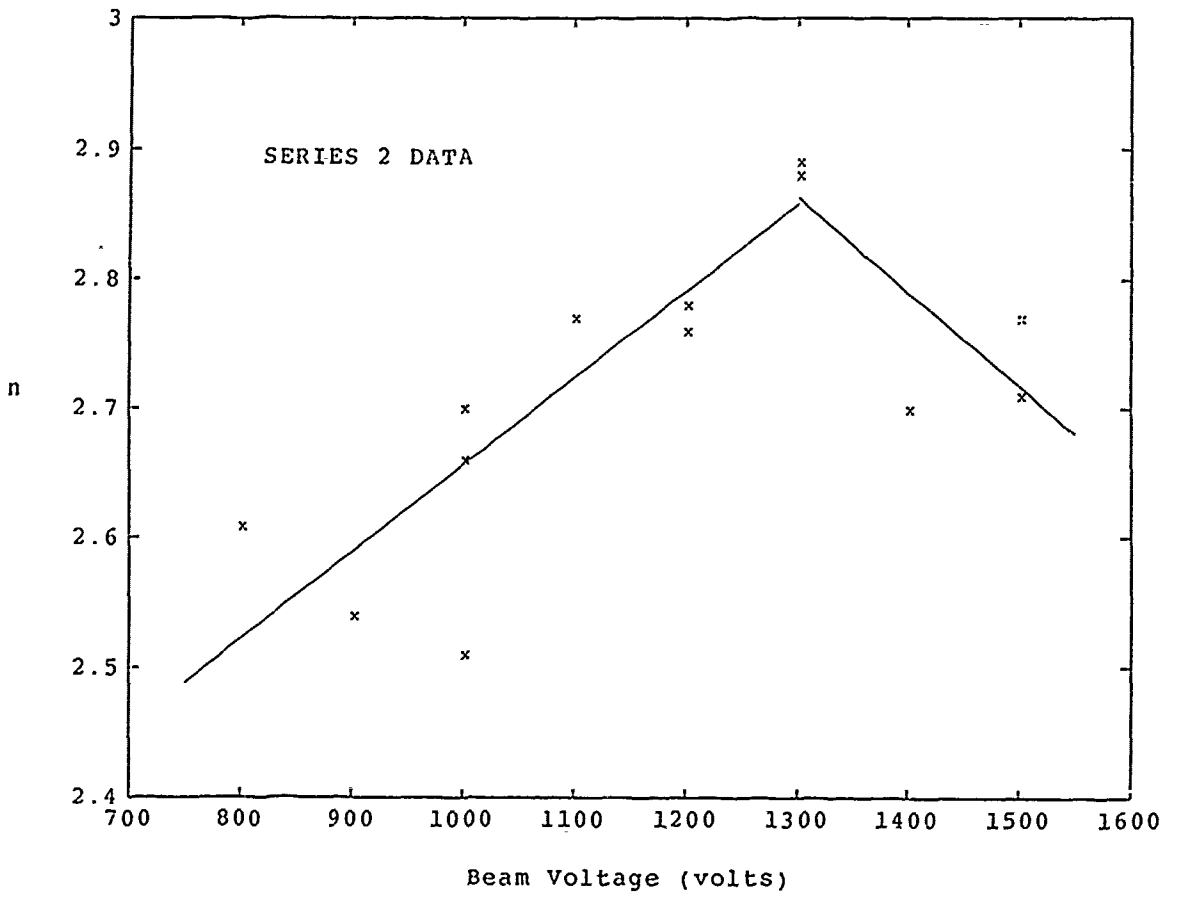

Figure 7. Refractive Index Change with Beam Voltage: Series 2

improved, uncertainty in the stability of the CH_4/Ar ratio was never better than 5%.

For the second series, changes with beam voltage were characterized. Figure 7 plots refractive index at 800 *nm* against beam voltage for runs during which the gas mix stayed constant. The linear fits are for beam voltages from 800V-1300V and 1300-1500V. Although somewhat scattered about the line, there is an apparent increase in the index with beam voltage up to 1300V. Above 1300V the trend appears to reverse. However, there is not enough data about the "break point" to characterize this apparent trend reversal. The lack of a clean trend in figure 7 is attributed to experimental error, particularly the stability of the deposition parameters.

Ellipsometry showed the extinction coefficients for these first two film series to be unexpectedly high across the spectrum. This fact was confirmed by spectrophotometric data showing transmission (after accounting for loss from the glass substrate) to be less than 70% at the longer wavelengths, and less than 50% for wavelengths shorter than 500 *nm*. The long term sputtered film for series two had a transmission of 40% at 800 *nm*, and less than 10% by 600 *nm*. This was unacceptable for a film only about 650 *nm* thick! As will be detailed in the next section, metal contamination was the main culprit.

The graphite shield used in the third series significantly reduced the films' absorption. Transmission was up to 80% from 500-800 *nm*, and the long term sputtered films were markedly improved. Figures 9 and 10 compare examples of transmission spectra from series 2 and 3. Oscillations in the spectra come from interference effects of the film.

The refractive index at 800 *nm* for the first two films in series 3 was less than 2.4. In an effort to get the refractive index back near the series 2 ranges, the CH_4/Ar ratio was stepped down. When the refractive index *also* went down, it became clear that sputtering from the graphite shield was affecting the deposition process. Only three films of this series were deposited with a constant CH_4/Ar ratio, that being about 15% less than series 2 films. Since this gas ratio was attained by holding the partial pressure of CH_4/Ar fixed and increasing the Ar flow, total operating gas pressure was 25% higher than the previous series. In essence, series 3 was a very different experiment.

Time being limited, only 7 films were successfully sputtered in series 3. The three that were grown with the same gas mix (films #50, #51, and #52) showed the same trend for refractive index and beam voltage (see figure 8). But what seemed to be simply confirmation of the results of series 2 turned out to be more than that, as RBS and ERD analysis revealed.

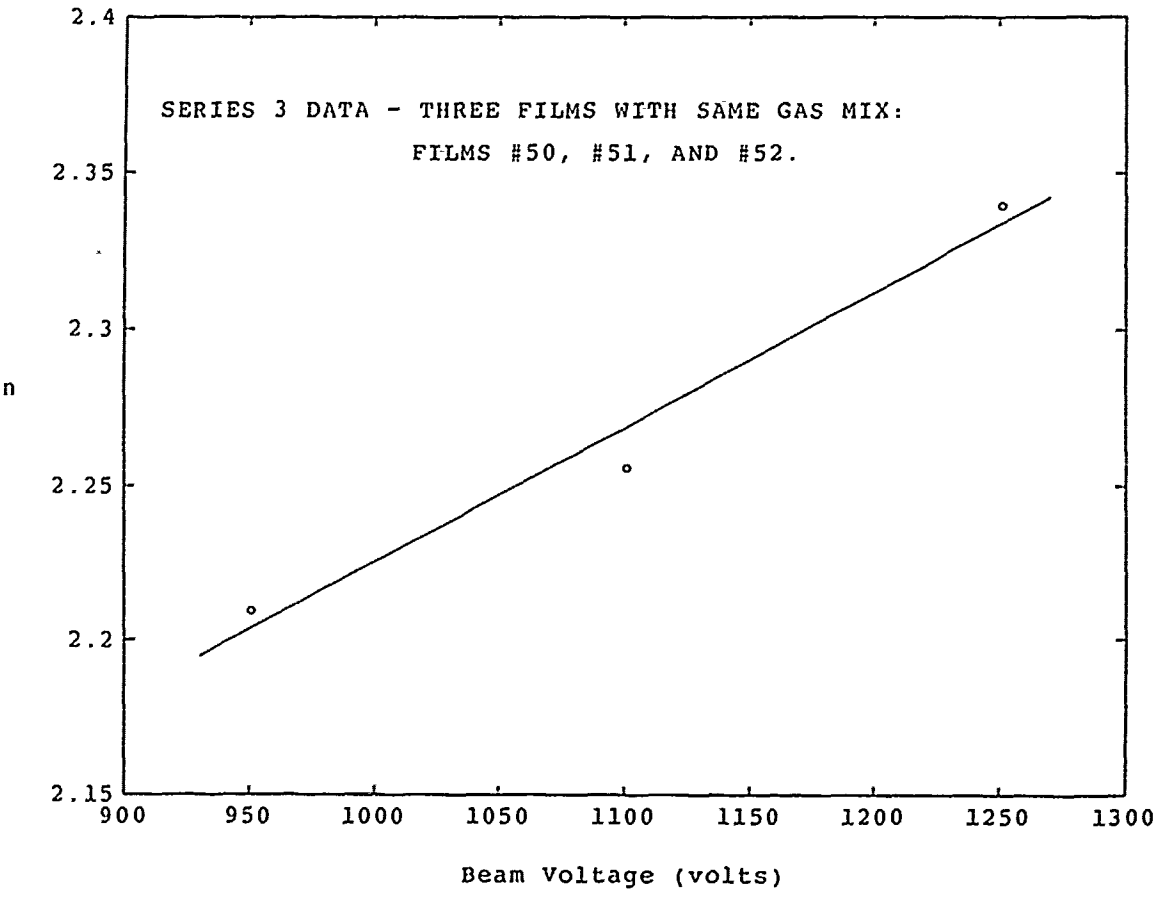

Figure 8. Refractive Index Changes with Beam Voltage: Series 3

4.3 Chemical Composition

A table of the RBS and ERD analysis can be found in appendix F. This table lists the percentages of each element, and the total mass density of the film. RBS data are available only for films #27 and higher since Be substrates were not used until then.

Looking at the big picture, the films show roughly equal amounts of Si, C, and H. The RMS average mass density for series 2 films is 2.04 ± .05 gm/cm^3, and for the three series 3 films grown with the same CH_4/Ar gas mix the average mass density was 1.79 ± .07 gm/cm^3. Metal contamination was reduced by an order of magnitude for the third series, confirming sputtering from the chamber walls (iron)

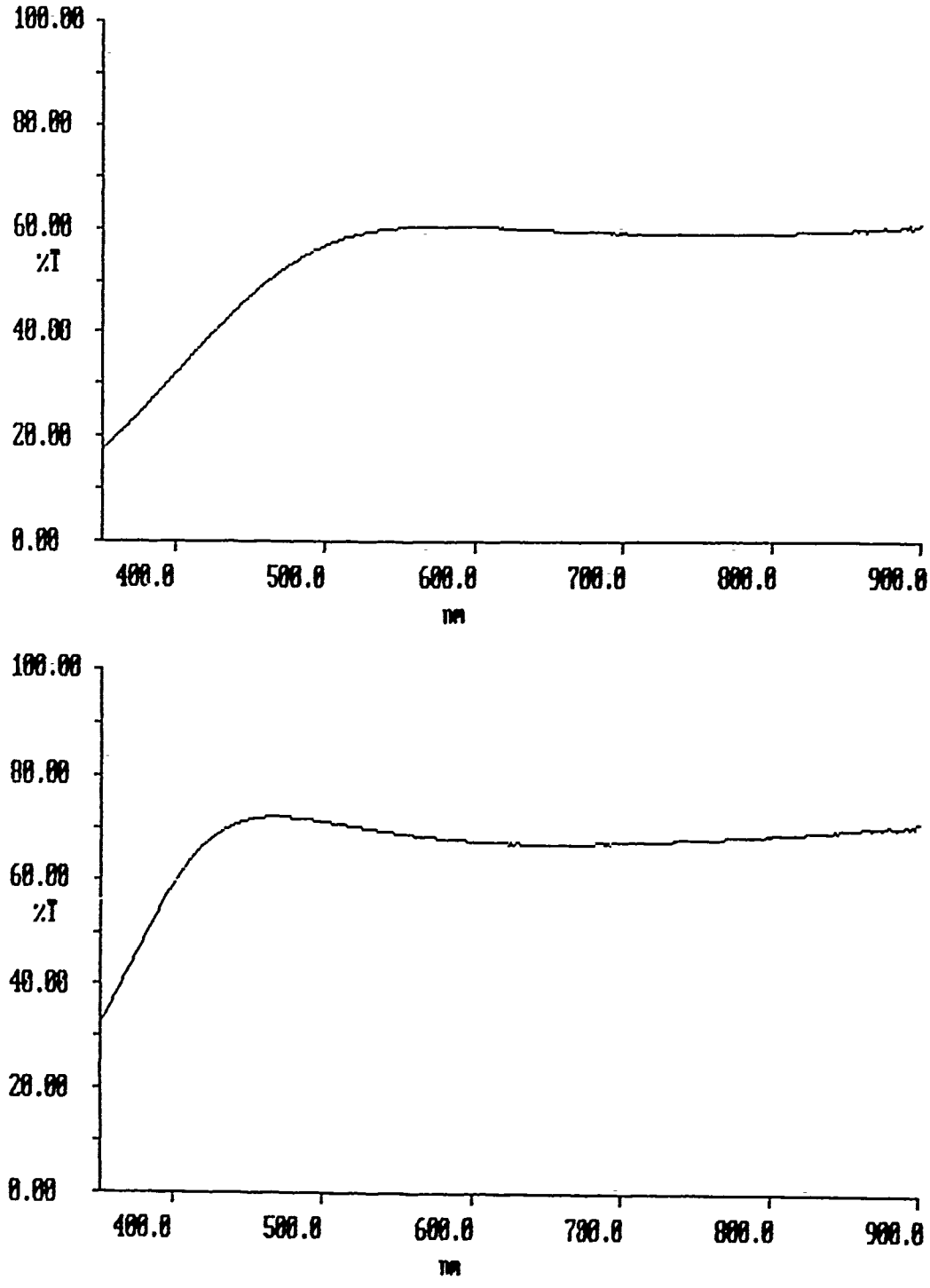

Figure 9. Series 2 and 3 Transmission Spectra for Films #42 (top) and #50 (bottom). Thicknesses are about $95nm$.

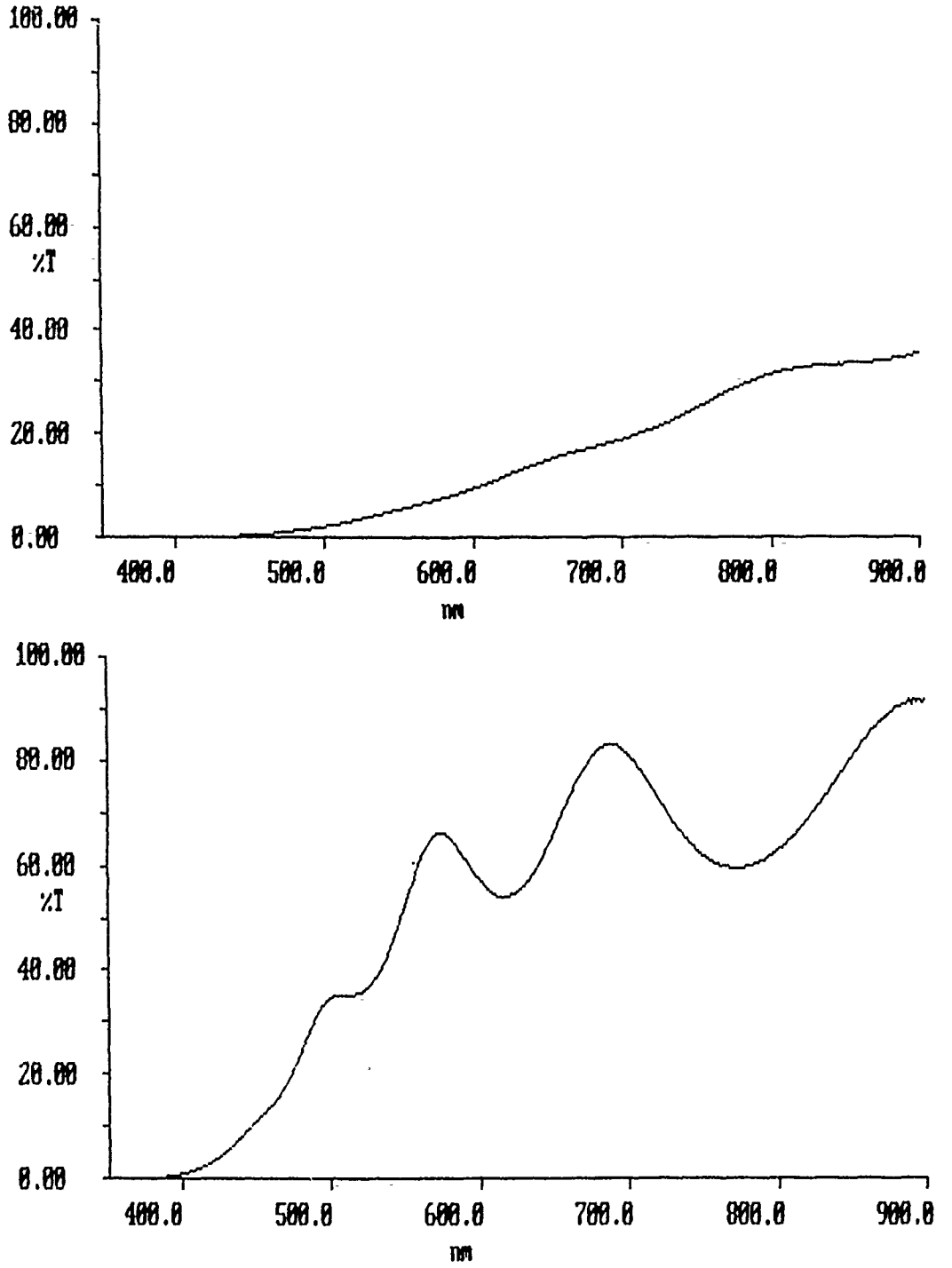

Figure 10. Series 2 and 3 Transmission Spectra for Films #44 (top) and #53 (bottom). Thicknesses are about $650nm$.

and welds in the cooling plumbing (silver). Tungsten content was nominally the same for all films, as expected. Since RBS was in three separate batches of films, the report on the last batch measured nitrogen counts, whereas the first two batches did not, reporting only "a hint of nitrogen in the films". The raw plots of RBS data runs (see appendix C for an example) show virtually identical curve shapes for the range of channels from which nitrogen counts were taken on the final batch. Since the oxygen content and RBS data plots for all films are similar, nitrogen counts must also be similar. Therefore, the nitrogen content for all films is assumed to be roughly the same.

From series 2 data, we learned that refractive index increases with increasing carbon and hydrogen content, as expected. Figure 11 shows refractive index plotted against the Si/C ratio.[1] It is important to note that films with higher carbon content also have more hydrogen. Hence, the Si/H content ratio plotted against refractive index (figure 12) shows the same trend as Si/C. This means the data from this study only shows how index of refraction changes when *both* carbon and hydrogen are increased *together*. So, the separate effects of each element cannot be clearly determined.

Deviations from the linear fit in figure 11 can be explained for a few points. For example, film #29 plots farthest from the line on the high side. But deposition conditions during that run were plagued by rapidly increasing acceleration grid current (another "thermal runaway" effect) which was mistakenly interpreted as a loss in net beam current. The beam current was increased manually throughout the run to compensate, getting as high as 25 mA. As was learned from the results for film #43 (25 mA beam current), the index of refraction increases markedly with beam current. Therefore, #29's deviation from the plot in figure 11 is due to experimental error. Farthest on the other side of the line is film #39. Because its mass density was

[1]Data points for films #40, #41, and #42 are not shown in series 2 plots because RBS data for these were not available.

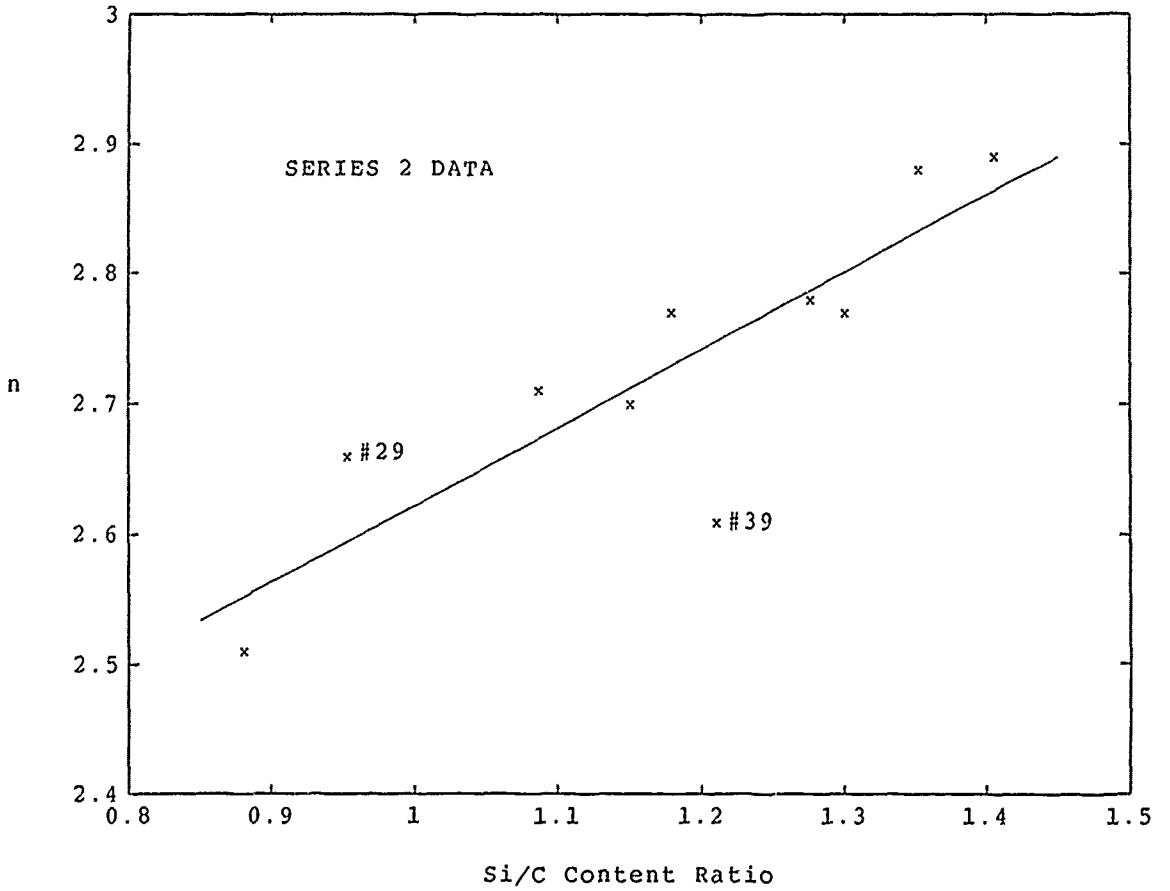

Figure 11. Refractive Index Changes with Si/C Content Ratio: Series 2

no different than that of the other films, #39's lower refractive index is attributed to much higher H content for the amount of C present, as shown in the plot of H/C content ratio against refractive index (figure 13). Also, film #39's somewhat higher oxygen content probably makes some contribution to its lower index of refraction.

Another especially interesting observation from figure 11 is that films grown with beam voltages greater than 1300V fall close to the linear fit near the center of the plot. This means that the trend reversal of figure 7 shows up here as a corresponding *decrease* in the Si/C ratio. There must be some process by which beam energies corresponding to beam voltages above 1300V caused these films to have *less* carbon and hydrogen.

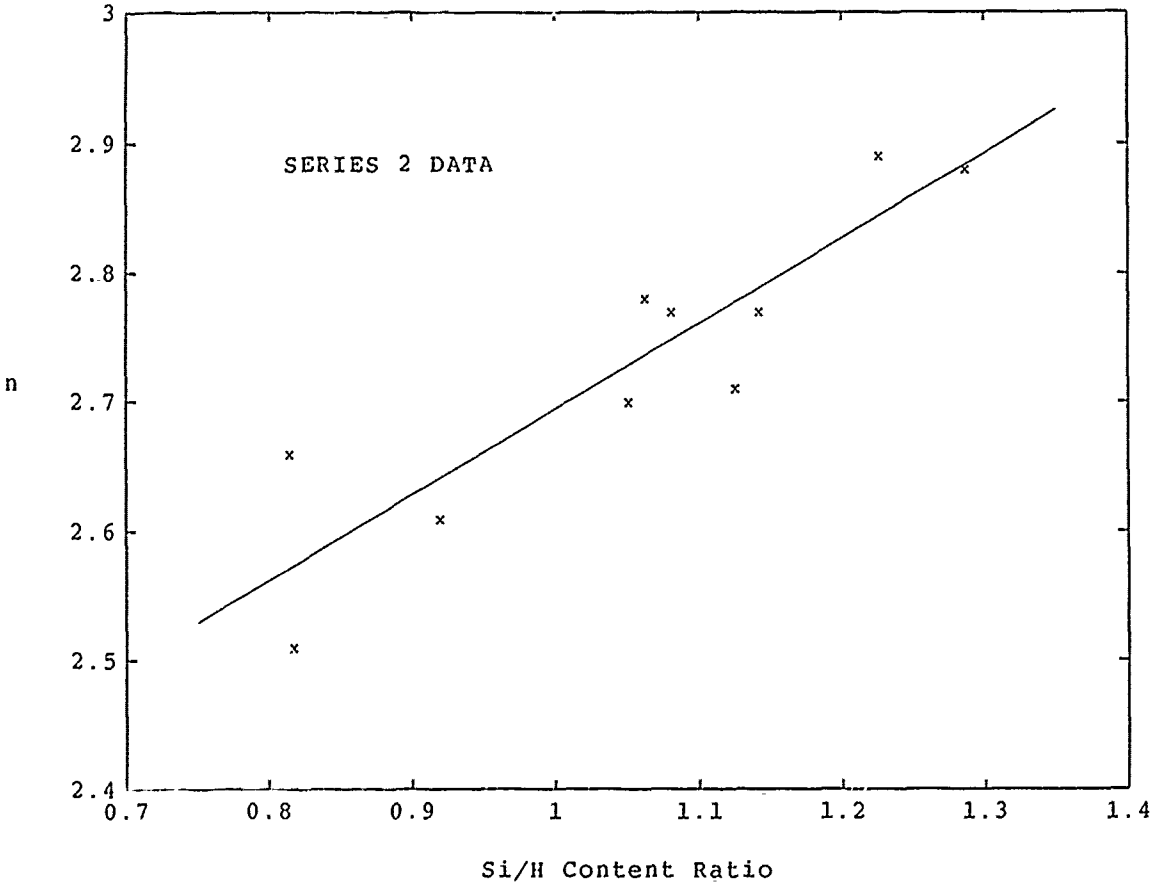

Figure 12. Refractive Index Changes with Si/H Content Ratio: Series 2

For series 3 films, the results were startlingly different. First, the graphite shielding reduced the films' metal content by an order of magnitude. This confirmed sputtering from surfaces left of the target. The next major difference was a lower index of refraction. This was not surprising since the added graphite (a source of sputtered carbon) was expected to increase the carbon content of the films. Looking at the gross features of refractive index, for comparable Si/C ratios the average indices for series 2 and 3 were 2.7 and 2.3, respectively. The average density of series 3 was less than series 2 by 10-15%. For a similar density difference between two ideal dielectrics, the Clausius-Mossotti relation predicts very nearly the same refractive index change as that between the average indicies of series 2 and 3 (30). Although this comparison to ideal dielectrics is much too simplistic, it does lend credence to

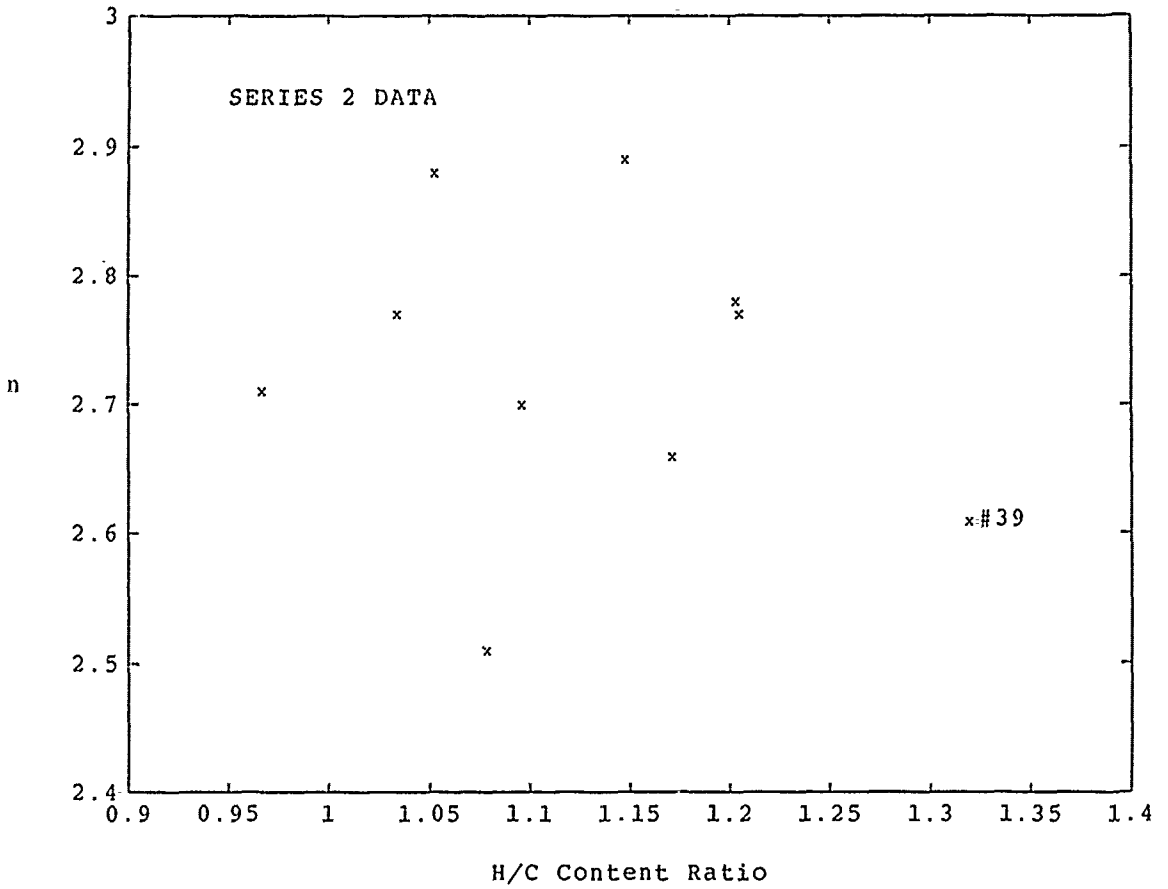

Figure 13. Refractive Index Changes with H/C Content Ratio: Series 2

the idea that differences in the absolute refractive indices between series 2 and series 3 films are in large measure due to the differences in density.

The refractive index for series 3 increased with beam voltage in like manner to series 2. But the index-Si/C trend for series 3 was *opposite* from series 2. Figure 14 shows the data from both series' for comparison. Remember that only three films of series 3 were deposited with the same methane-argon gas mix (those of figure 8), those are the three used for linear fit shown in figure 14 for series 3 data.

This opposite trend in Si/C content ratio with refractive index is quite a curious result, and must have occurred because of the graphite shield. In fact, because the shield was being sputtered series 3 was in effect a whole new experiment: the sputtering of two "targets" simultaneously. Sputtered efflux from the graphite must

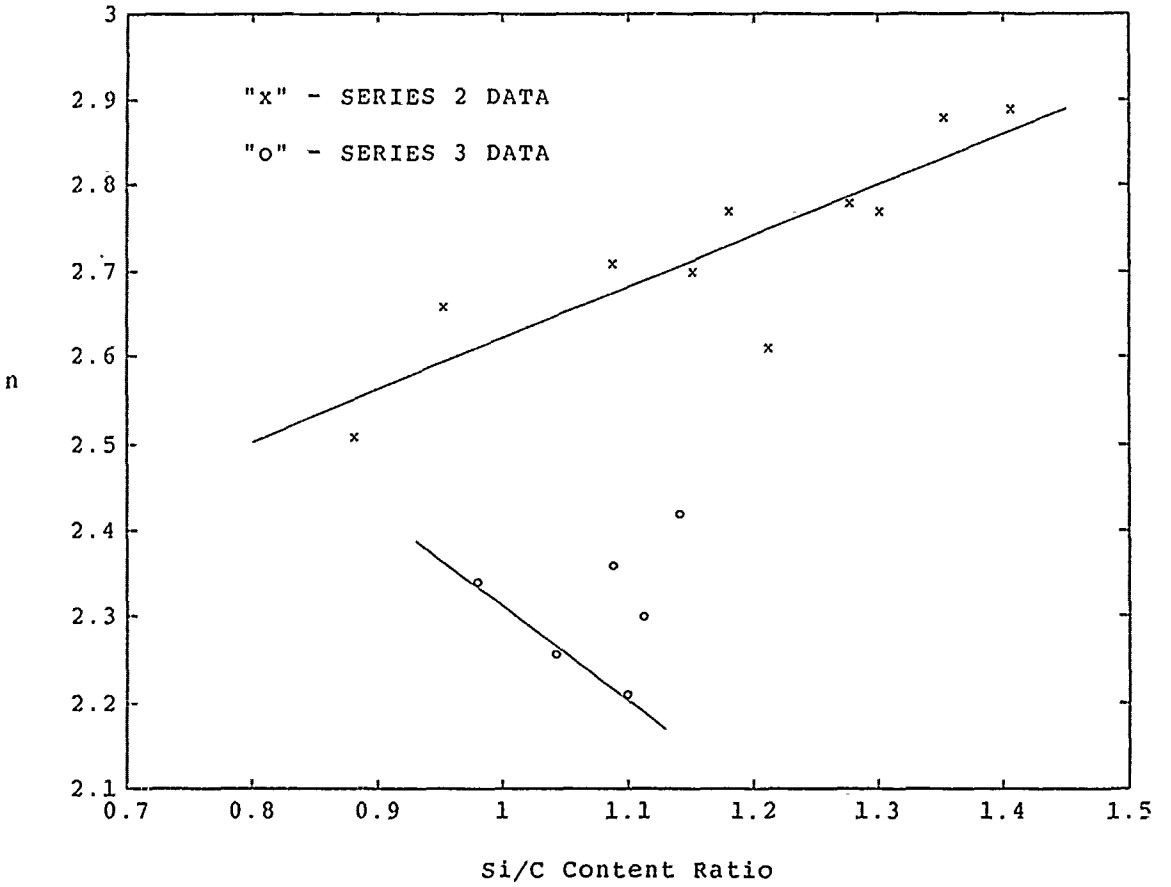

Figure 14. Refractive Index Changes with Si/C Content Ratio: Series 2 & 3

have increased with beam voltage, just as observed for the Si target (higher deposition rate at higher beam voltage). Due to the shield's location and orientation in the chamber, carbon from the graphite was sputtered onto *both* the film *and* the Si target at a rate increasing with beam voltage. The deposition of this additional carbon onto the growing film would bring the Si/C ratio down as the beam voltage increased.

Although this explanation is reasonable, it does not explain why the refractive index *increased* with beam voltage when the Si/C ratio *decreased.* Not enough data is available to give a justifiable explanation for this result. But, it is apparent that sputtering graphite and silicon together complicated the dynamics of the sputtering process enough to change the nature of film growth.

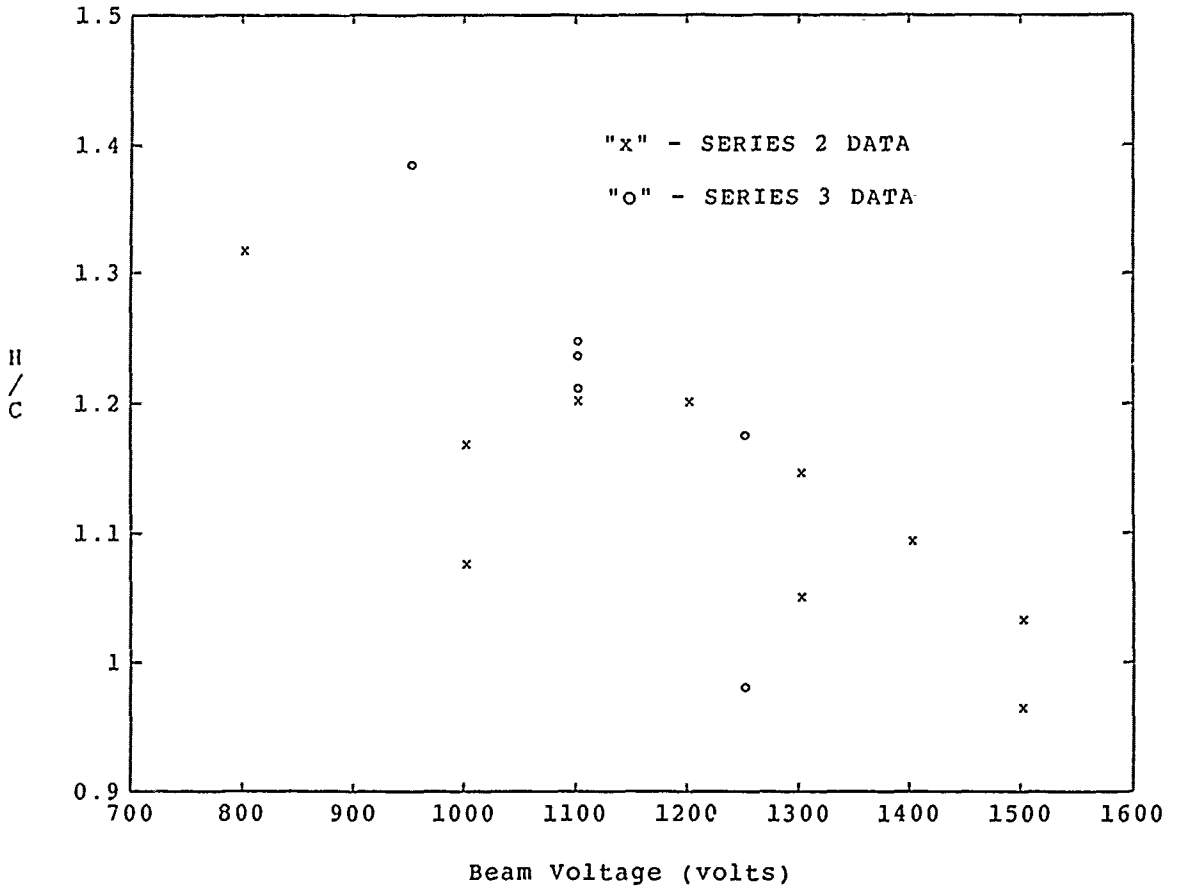

Figure 15. H/C Content Ratio Changes with Beam Voltage: Series 2 & 3

Another result worth noting is how the hydrogen to carbon content ratio changed with beam voltage. Figure 15 combines series 2 and 3 data to show how H/C content ratio generally decreases with increasing beam voltage. It is possible that this decrease in H for the amount of C in the film is due to the increased energies of the sputtered efflux with higher beam voltages. Notice also that series 2 and 3 data are not "split" as in figure 14, and series 2 shows no trend reversal as in figure 7. This indicates that the incorporation of H into the film depends significantly on the amount of carbon sputtered into the film.

4.4 Physical Characteristics

Physical characteristics of the films were obtained by visual inspection, using ellipsometry results (film thickness), and atomic force microscopy. Visually, the films adhered well to silicon substrates regardless of thickness. The only deterioration of films on silicon occurred for those substrates swabbed with methanol before deposition, already attributed to a residual impurity from the methanol. Curling and flaking from glass and Be substrates occurred only for the long term sputtered films. On those, more than 50% of the area of each thicker film was intact, with one or two badly flaked areas. Because the Be foil was not polished, its surface was visibly rough. This was a problem only for the thicker films, which were badly flaked over the entire surface. All areas of the films which adhered well initially looked just as good many weeks later, and ellipsometry data was unchanged over the same time.

For films grown left of the quartz crystal, film thickness varied 10% from one side of the film to the other (about 2cm). Films from the crystal's location were more uniform, with less than 3% variation across the same distance. This again highlight the decreased deposition rate away from ion-beam axis.

Except for a uniform population of 0.1μm dust particles about 1μm apart, the surface was flat and featureless. Average roughness over a 36 μm^2 area was 2.2 nm, and over a 6μm cross section was 0.8 nm.

V. Conclusions and Recommendations

This chapter summarizes what was learned about ion-beam sputtered a:SiC_x:H films, and presents recommendations for follow-on work.

5.1 Conclusions

Using an ion-beam to sputter thin films with continuously varying refractive index profiles, or selecting deposition conditions to produce a single desired index, should be possible. The results show that index increases monotonically with beam energy up 1300V beam voltage, then the index decreases with higher beam voltages. The fact that a monotonic trend exists makes beam voltage a possible design parameter. But control of the deposition conditions was not precise enough to fully characterize the method. The fact that the ion-beam's outer edges sputtered more than the intended target highlights the most important conclusion: All ions emanating from the ion source must be properly contained.

Although both series 2 and series 3 films show the same relationship between refractive index and beam voltage, the trends for index and Si/C content ratio are opposite. This is a direct result of changes in sputtering conditions between the two series, the installation of a graphite shield for series 3 being the major difference. The films' atomic makeup also depends greatly on what surfaces are being sputtered (chamber walls, graphite shield, silicon target) as well as the stability of deposition conditions. The largest deviations from trends can, in individual cases, be explained by poor control of deposition conditions or higher than average hydrogen content. Greater hydrogen content seemed to decrease the refractive index.

5.2 Recommendations

Here are recommendations for follow-on experiments with ion-beam sputtered films:

- Complete control of the ion-beam is paramount.
- Gas flow to the ion source must be controlled in a steady, repeatable manner.
- Target and substrate should be arranged to maximize deposition rate.
- Reactive gases that minimize deterioration in ion source performance should be tried.
- Infrared spectra of these films should be analyzed to determine chemical bonding arrangements.

The first item is the most important. Energetic ions at wide divergence angles from the source will sputter unacceptable impurities into the films. If the target does not catch all the ions, a baffle must be placed between the ion source and the target so as to block the outer edges of the beam. Any such baffle must also be placed so sputtering from the baffle itself does not contaminate the film.

Almost as important as ion-beam control is control of the gas flow to the ion source. Mass flow controllers are a must for precise and steady flow control. Mass flow monitors would help, but if a less sensitive valve arrangement is not possible, stability during the run will not improve.

If this technique is ever to achieve growth of films microns thick, the deposition rate must be maximized. A larger vacuum chamber cavity, and mounts for the target and substrate that are adjustable during a run would be ideal. Anything would be an improvement.

Increasing the endurance of the ion source depends greatly on the reactive gas used. Replacing CH_4 with CF_4 is planned for future experiments studying beam voltage effects. Another idea is to sputter a composite target of silicon and carbon (like SiC crystal) with a hydrogen/argon ion-beam. This would remove carbon from the internal working of the ion source altogether, eliminating carbon deposits from the source's insulators, but retain all the ingredients for a-SiC_x:H thin films.

Finally, the films produced in this study have untapped information to offer. Specifically, the infrared absorption spectra can reveal the relative number of chemical bond types, which may shed light on data trends not resolvable by other means.

Appendix A. Procedure Used to Set and Measure Gas Partial Pressures

Here is a list of the procedure developed during this study for setting and measuring the partial pressures of CH_4 and Ar gases for a typical experimental run. It is important to emphasize that patience in allowing the pressures to stabilize after each change in gas flow is required for accurate settings and measurements of the partial pressures.

1. After pre-cleaning, shut off the Ar gas valve and allow the chamber to evacuate to about 1×10^{-6} torr (no Ar^+ peak on the mass spectrometer).
2. Open the CH_4 valve and set the pressure on the ionization gauge to the desired indication. For these experiments it was in the $6.2\text{-}7.5\times10^{-5}$ torr range. Allow the pressure to stabilize a few minutes.
3. Open the Ar valve and set the pressure on the ionization gauge to the desired indication. For this experiment, it was in the $1.0\text{-}1.4\times10^{-4}$ torr range. Allow pressure to stabilize.
4. Observe the peak heights of CH_4^+ and Ar^+ on the mass spectrometer. For first time runs, record the ratio of the peak heights. If setting the gas mix to match a previous run, adjust the Ar gas valve to make the peak heights the same ratio as before, and let it stabilize.
5. Check the ratio of the peaks as often as desired/allowed during the run by turning the ion source off, since the peaks on the mass spectrometer change dramatically with the ion source on.
6. When the run is finished, record the ratio of the mass spectrometer peaks. Shut off the Ar gas valve, let the pressure stabilize, and record the CH_4 pressure. Compare this with the initial CH_4 partial pressure to check stability during the run.

7. Open the Ar valve and set the mass spectrometer peak heights back to the same ratio recorded at the end of the run, letting the settings stabilize to insure the correct mix.

8. Shut off the CH_4 valve, allow the pressure to stabilize, then record the Ar pressure. This was the Ar partial pressure for the run.

Appendix B. **Ellipsometry**

Ellipsometry is the measurement of the change in polarization of light after reflection from (or transmission through) a sample. Using complex notation, the oscillating electric field of an electromagnetic plane wave can be written

$$E = E_o e^{j\delta}$$

where E_o is the amplitude of the electric field, and δ is its phase. Any electric field vector can be resolved into two components along two orthogonal directions in the wave front, say x and y. Then the *relative* amplitude and *relative* phase of one component to the other can be expressed as

$$\chi = \frac{\mid E_y \mid}{\mid E_x \mid} e^{j(\delta_y - \delta_x)}$$

For light reflected off a surface, the electric field is normally defined by p (in the plane of incidence) and s (perpendicular to the plane of incidence) directions. Then, the relative amplitudes and phases in terms of the overall complex Fresnel reflection coefficients (R) of a thin film on a substrate are

$$\frac{E_{rp}}{E_{ip}} = R_p = \mid R_p \mid e^{j\Delta_{Rp}}$$

$$\frac{E_{rs}}{E_{is}} = R_s = \mid R_s \mid e^{j\Delta_{Rs}}$$

where i stands for incident wave. Reflection ellipsometry is based on measurements of the *ratio* of these polarization states for the incident and reflected waves. This ratio is simply

$$\rho = \frac{R_p}{R_s}$$

which is more commonly expressed as,

$$\rho = tan\psi e^{j\Delta}$$

where

$$tan\psi = \frac{|R_p|}{|R_s|}$$

$$\Delta = \Delta_{Rp} - \Delta_{Rs}$$

The ellipsometric data is numerically expressed as $tan\psi$ and $cos\Delta$. For more detailed information on ellipsometry theory and applications, see reference (31).

Figures 16 and 17 show sample plots of ellipsometric data and the computer fit for film #20. The values for refractive indices and extinction coefficients are given in tables 5 and 6.

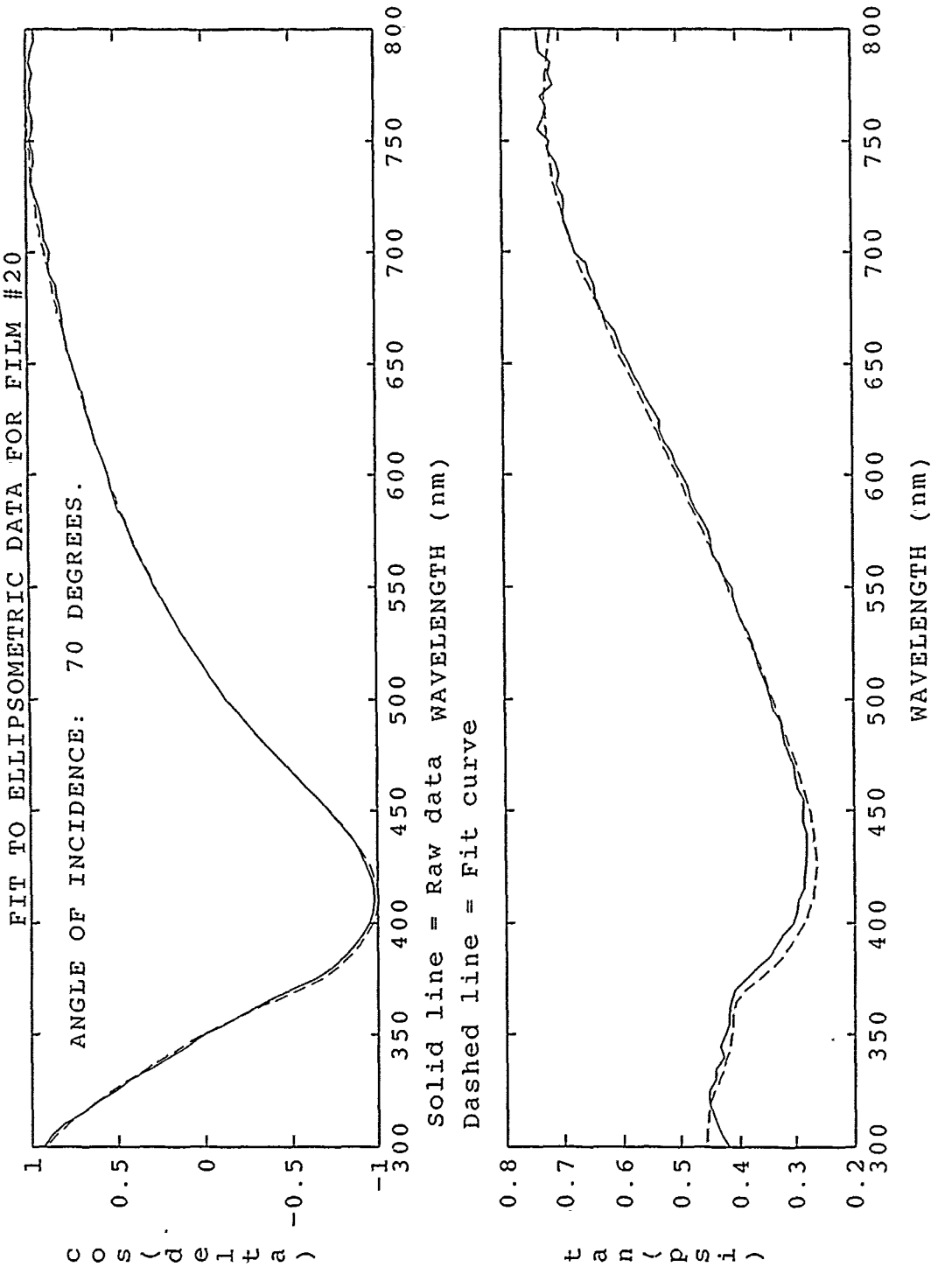

Figure 16. Sample of raw and fitted ellipsometric data for film #20 at a single angle of incidence for the ellipsometer's light beam.

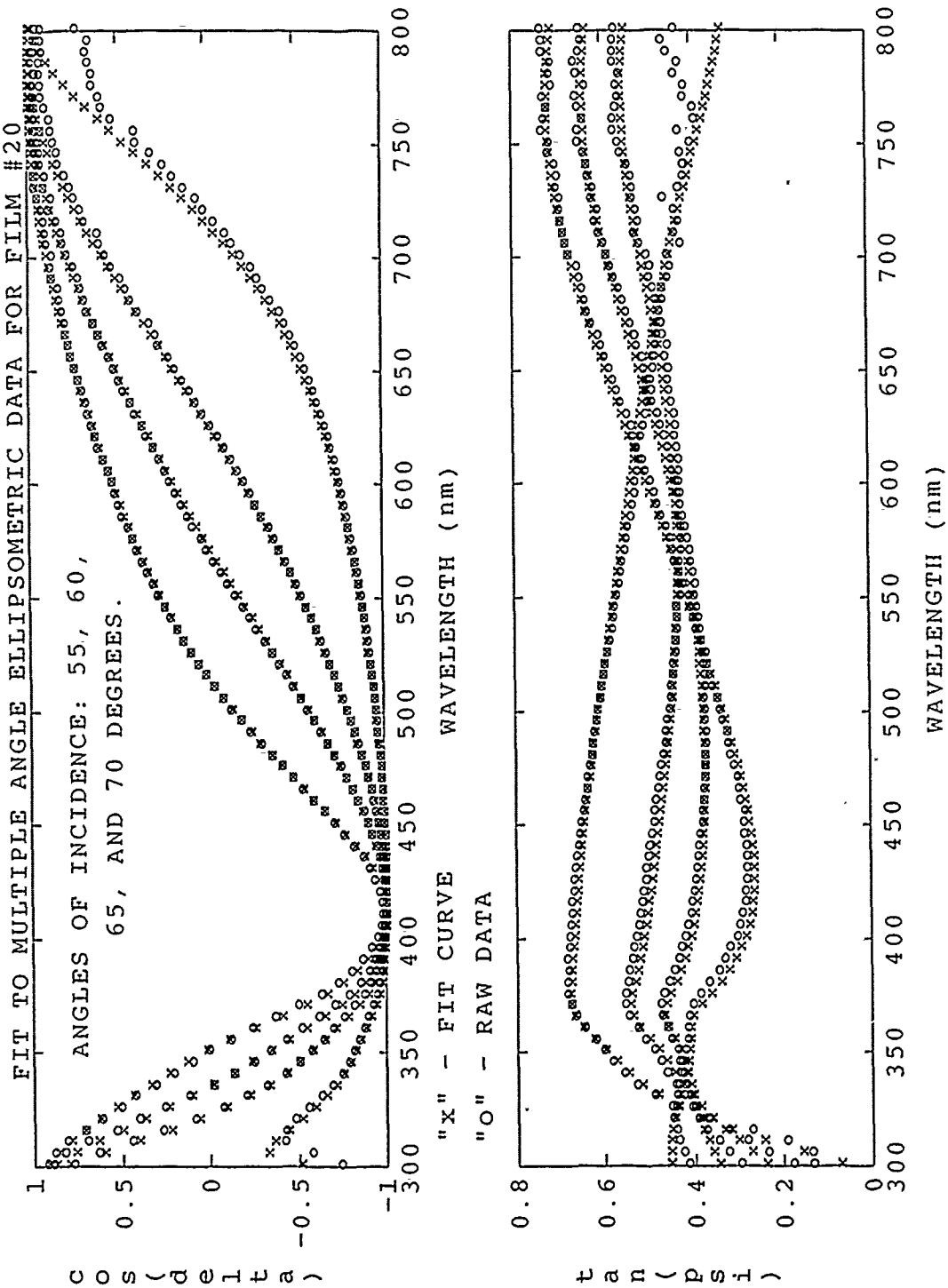

Figure 17. Sample of raw and ellipsometric data for film #20 showing four different angles of incidence for the ellipsometer's light beam.

Appendix C. Rutherford Backscatter Spectrometry (RBS) and Elastic Recoil Detection (ERD)

As an analytical technique, RBS is easy to understand and apply since it is based on classical scattering in a central-force field. Helium ions (He^+) are bombarded against the sample and the energies of scattered He^+ ions are measured. Collisions with heavy nuclei in the sample result in little energy loss, while collisions with lighter elements reduce the reflected ion's energy. The energy spectrum of scattered He^+ contains information on the type and relative amounts of elements in the sample.

For accurate analysis of elements in a thin film, the substrate must be a material (normally a single element) with an atomic number lower than the elements in the film. Thus, He^+ ions scattered by the film will have energies higher than ions scattered by the substrate, and show distinct peaks on the energy spectrum. This is why accurate RBS analysis of the lightest elements is difficult, as their energy peaks are buried in the high number of He^+ counts due to the substrate.

Figure 18 shows one plot from an RBS measurement of one of the a-SiC_x:H films from this study. The "Channel" axis is the energy axis, and the "Counts" axis is the number of He^+ ions detected. The width of a peak is due to energy lost as the bombarding ion penetrates the film. The right side of the peak are counts from atoms near the surface of the film, and the left side from atoms near the substrate's surface. The counts to the far left (less than 150) are from the substrate material, in this case beryllium, and elements in the film and substrate lighter than beryllium.

Since heavy ions colliding with lighter nuclei only scatter forward, a different method must be employed to determine hydrogen content of a thin film. ERD does just that by scattering He^+ ions off the sample at a glancing angle (typically 15°) and measuring the energy spectrum. Using this method, depth profiles for hydrogen

and deuterium in the same film can be accurately determined. For more information on RBS and ERD see reference (32).

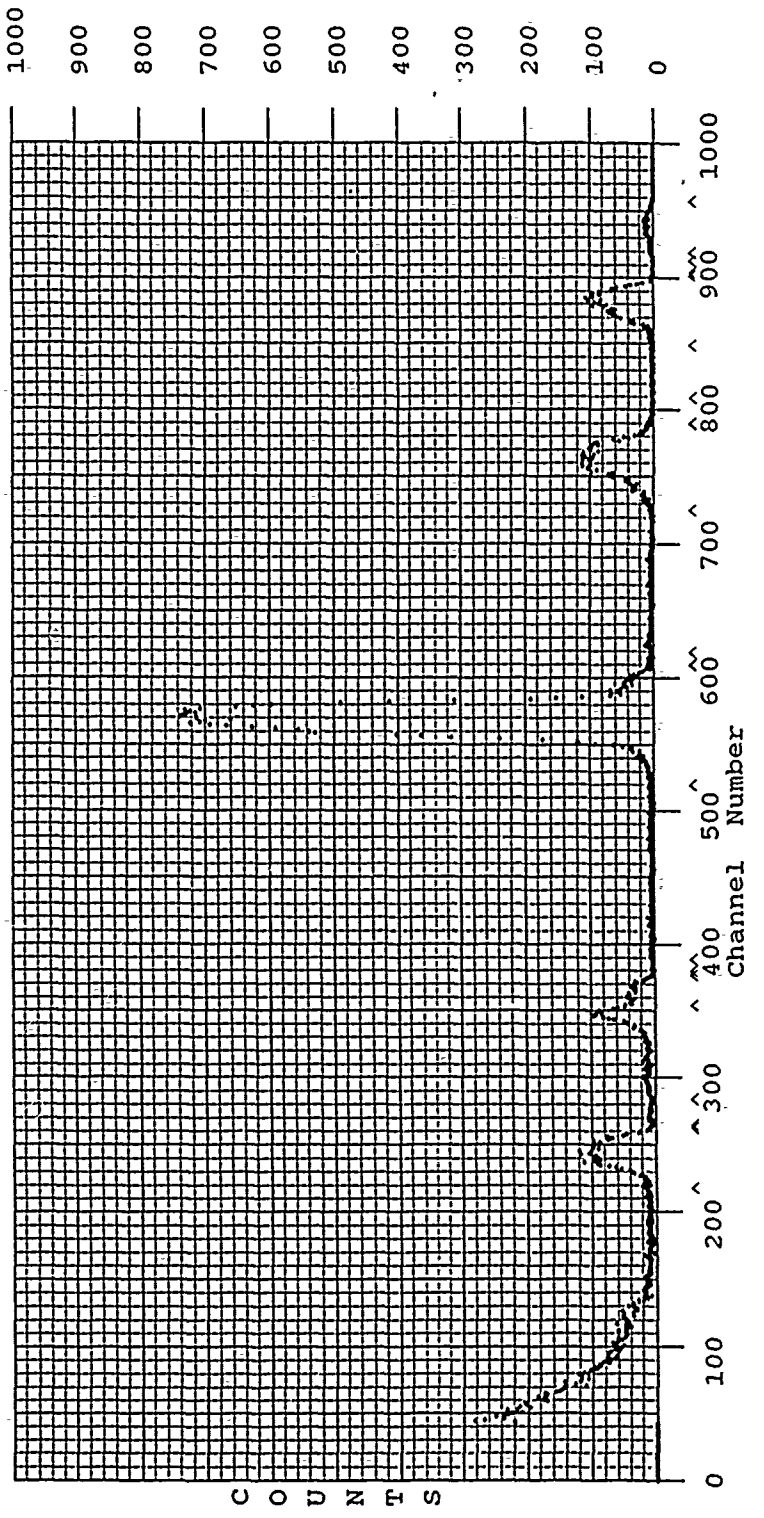

Figure 18. Sample Copy of RBS Data Plot

Appendix D. **Deposition Parameters**

The following tables list the important deposition parameters for each successful experimental run. Items with a dash ("-") were not recorded.

Pressures reported here are *indicated* pressures on an ionization gauge calibrated with nitrogen.

The procedures for recording partial pressures of CH_4 and Ar *changed significantly* from series 1 to series 2 & 3, hence the differences in reported pressure readings between table 2 and tables 3 & 4. Pressures for films #28 and beyond are values at the *end* of the run. The two numbers in the "Total" pressure column are for the ion source "OFF/ON."

Table 2. Deposition Parameters: Series 1

FILM#	PRESSURES ($\times 10^{-5}$ torr)			ION SOURCE (volts)	(mAmps)
	CH_4	Ar	Total	(volts)	(mAmps)
17	8	8	16	1500	22
18	4	12	16	1500	22
19	6	10	16	1500	21
20	10	6	16	1500	25
24	8	8	16	1500	20
26	8	8.0	15-16	1500	20

Table 3. Deposition Parameters: Series 2

FILM#	PRESSURES ($\times 10^{-5}$ torr)			ION SOURCE	
	CH_4	Ar	Total	(volts)	(mAmps)
28	6.9	-	12/-	1300	20
29	6.4	-	11/7.5	1000	20
30	6.5	-	11/7.6	1500	22
32	6.3	-	11/7.1	1500	21
33	6.2	-	10/6.7	1000	21
34	6.5	-	11/7.1	1400	21
35	6.4	-	11/7.3	1300	21
36	6.7	-	11/7.1	1300	21
37	6.7	-	11/7.0	1200	20
38	6.5	4.8	11/7.0	1100	20
39	6.2	4.5	10/6.5	800	21
40	6.6	5.1	11/7.2	1000	20
41	6.6	5.1	11/7.2	1200	20
42	6.9	5.2	12/7.4	900	20
43	6.8	5.1	11/7.3	1000	25
44	6.7	4.8	11/6.9	1050	20

Table 4. Deposition Parameters: Series 3

FILM#	PRESSURES ($\times 10^{-5}$ torr)			ION SOURCE	
	CH_4	Ar	Total	(volts)	(mAmps)
45	6.5	4.4	11/6.5	1100	21
46	6.8	4.7	11/7.1	1250	21
47	6.9	5.3	12/8.0	1100	21
50	7.0	6.0	13/8.9	1100	21
51	7.1	6.2	13/9.2	950	21
52	7.1	6.4	13/9.6	1250	21
53	6.6	6.2	12/9.0	1100	21

Appendix E. Refractive Indices, Film Thicknesses, and Extinction Coefficients

These tables list indices of refraction, film thicknesses, and extinction coefficients obtained from curve fitting the ellipsometry data.

The uncertainty for n(800nm) and thickness (d) for series 2 & 3 is less than 1%, and less than 4% for the other two indices. The estimated error for k(700nm) is 3% with other extinction coefficient (k) values having uncertainties of 15% or more. The fact that some k values are reported as negative is attributed to uncertainty in extinction coefficients that have values very nearly equal to zero.

Table 5. Refractive Indices and Film Thicknesses: Series 1

FILM#	n(800nm)	n(600nm)	n(400nm)	d(nm)
17	2.40	2.52	2.69	71.0
18	3.80	3.94	3.94	132
19	3.11	3.25	3.40	92.0
20	2.16	2.21	2.31	96.6
24	2.58	2.69	2.84	77.0
26	2.69	2.78	2.81	77.0

Table 6. Extinction Coefficients: Series 1

FILM#	k(300nm)	k(400nm)	k(500nm)	k(550nm)	k(700nm)
17	0.34	-	.038	-	-
18	-	1.65	-	0.85	0.47
19	0.11	-	0.18	-	-
20	.208	-	0	-	-
24	.381	-	.090	-	-
26	0.38	-	.213	-	-

Table 7. Refractive Indices and Film Thicknesses: Series 2

FILM#	n(800nm)	n(600nm)	n(400nm)	d(nm)
28	2.42	2.50	2.59	86.0
29	2.66	2.73	2.84	87.2
30	2.77	2.83	2.93	88.8
32	2.71	2.75	2.81	89.5
33	2.51	2.55	2.60	96.0
34	2.70	2.77	2.85	89.0
35	2.88	2.93	2.98	89.0
36	2.89	2.97	3.08	92.0
37	2.78	2.84	2.93	90.3
38	2.77	2.83	2.94	96.0
39	2.61	2.67	2.77	92.5
40	2.70	2.78	2.90	98.0
41	2.76	2.83	2.93	97.0
42	2.54	2.60	2.72	96.0
43	2.82	2.88	2.99	94.0

Table 8. Extinction Coefficients: Series 2

FILM#	k(300nm)	k(400nm)	k(500nm)	k(550nm)	k(700nm)
28	.427	-	.090	-	-
29	-	.361	-	.146	.053
30	-	.520	-	.191	.046
32	-	.459	-	.169	.042
33	-	.306	-	.102	.019
34	-	.431	-	.137	.0069
35	-	.609	-	.254	.095
36	-	.600	-	.272	.132
37	-	.457	-	.197	.080
38	-	.498	-	.174	.041
39	-	.330	-	.093	.0033
40	-	.430	-	.107	-.020
41	-	.470	-	.186	.043
42	-	.328	-	.108	.0043
43	-	.550	-	.241	.110

For series 3, three runs had substrates located placed in both locations; left of and centered on the quartz crystal. Films from the left location have the suffix "L", and films from the center,"C".

Table 9. Refractive Indices and Film Thicknesses: Series 3

FILM#	n(800nm)	n(600nm)	n(400nm)	d(nm)
45L	2.39	2.48	2.66	87.3
45C	2.30	2.33	2.52	115
46L	2.40	2.52	2.72	79.8
46C	2.36	2.42	2.61	98
47L	2.49	2.60	2.81	88.2
47C	2.42	2.49	2.73	114
50	2.26	2.32	2.43	95.0
51	2.21	2.26	2.37	98.0
52	2.34	2.40	2.53	99.0

Table 10. Extinction Coefficients: Series 3

FILM#	k(400nm)	k(550nm)	k(700nm)
45L	.199	-.015	-.058
45C	.158	-.016	-.012
46L	.194	-.007	-.041
46C	.216	.015	-.038
47L	.273	.015	-.062
47C	.335	.046	-.029
50	.119	.006	.003
51	.136	.004	.004
52	.190	.029	.008

Appendix F. Atomic Composition Data

The tables below, for series 2 and 3, show the atomic percent of each element listed and the total mass density (md) for the film. All data for films of series 3 is on center (quartz crystal location) mounted substrates.

RBS analysis for series 3 films included counts for nitrogen, not done for series 2. Examining the raw RBS plots, it is safe to assume that nitrogen content for series 2 was roughly equivalent to series 3. Uncertainties are 5% for at%, and 6% for mass density.

Table 11. Atomic Percentages and Mass Density: Series 2

FILM#	Si	C	H	O	Fe	Ag	W	md(gm/cm^3)
28	27.0	32.5	35.2	2.9	1.6	.68	.022	1.95
29	29.2	30.7	36.0	1.6	1.6	.85	.008	2.01
30	35.2	29.9	30.9	1.7	1.7	.45	.006	2.09
32	33.4	30.8	29.7	3.0	2.5	.56	.008	2.09
33	28.3	32.2	34.7	2.4	2.1	.41	.009	1.94
34	33.4	29.1	31.8	2.9	2.3	.53	.011	2.05
35	37.3	27.7	29.1	2.7	2.5	.74	.010	2.04
36	37.6	26.8	30.7	2.2	2.2	.54	.011	2.07
37	34.8	27.3	32.8	2.7	1.9	.43	.008	2.10
38	35.3	27.2	32.7	2.9	1.5	.36	.009	2.07
39	32.3	26.7	35.2	3.9	1.6	.34	.015	2.03
43	37.0	24.0	33.4	3.0	2.0	.50	.016	1.94

Table 12. Atomic Percentages and Mass Density: Series 3

FILM#	Si	C	H	N	O	Fe	Ag	W	md(gm/cm^3)
45C	31.4	28.3	35.3	2.0	3.3	.15	.003	.005	1.86
46C	34.1	31.4	30.8	1.6	1.9	.21	.050	.005	1.97
47C	32.9	28.9	35.0	1.4	1.6	.16	.034	.006	2.01
50	30.0	28.8	35.6	2.7	2.8	.09	.009	.002	1.82
51	30.2	27.6	38.1	1.8	2.1	.15	.009	.004	1.69
52	29.8	30.5	35.9	2.2	1.4	.13	.017	.002	1.85

Bibliography

1. Catherine, Y., and A. Zamouche. "Ion Bombardment Effects in Plasma Deposition of Hydrogenated Amorphous Silicon Carbide Films: A Comparative Study of D.C. and R.F. Discharges," *Thin Solid Films, 109*, (1983), p145.
2. Wei-Liang Lin, et al. "Identification of Infrared Absorption Peaks of Amorphous Silicon-Carbon Alloy by Thermal Annealing," *Applied Physics Letters, 51*, (1987), p2112.
3. Murphy, A. R. "Fabrication of Rugate Filters By Co-Deposition of Lanthanum Fluoride and BArium Fluoride," AFIT GEP-88D-5, Master's Thesis, (Unpublished), (1988).
4. Johnson, W. E. "An Overview of Rugate Filter Technology," *Optical Interference Coatings: 1988 Technical Digest Series, 6*, (1988), p118.
5. Gunning, W., et al. "Codeposition of Continuous Composition Rugate Filters," *Optical Interference Coatings: 1988 Technical Digest Series, 6*, (1988), p126.
6. Gunning, W. "Gradient-Index Thin Films: An Emerging Optical Coating Technology," *SPIE Vol. 1019 Thin Film Technologies III*, (1988), p204.
7. Semenov, A. P. "Thin-Film Deposition by Ion-Beam Sputtering (Review)," *Instruments and Experimental Techniques, 33* (Translated from Russian), (1990), p735.
8. Parsons, R. "Sputter Deposition Processes," *Thin Film Processes II*, edited by John L. Vossen and Werner Kern. Academic Press, 1991.
9. Harper, J. M. E. "Ion Beam Deposition," *Thin Film Processes*, edited by John L. Vossen and Werner Kern. Academic Press, 1978.
10. Martin, P. J. and R. P. Netterfield. "Optical Films Produced by Ion-Based Techniques," *Progress in Optics XXIII*, edited by E. Wolf, Elsevier Science Publishers B.V., 1986.
11. Rossnagel, S. M. "Glow Discharge Plasmas and Sources for Etching and Deposition," *Thin Film Processes II*, edited by John L. Vossen and Werner Kern. Academic Press, 1991.
12. Chatam, H., et al. "Total and Partial Electron Collisional Ionization Cross Sections for CH_4, C_2H_6, SiH_4, and Si_2H_6," *Journal of Chemical Physics, 81*, (1984), p1770.
13. Bleakney, W. "Ionization Potentials and Probabilities for the Formation of Multiply Charged Ions in Helium, Neon, and Argon," *Physical Review, 36*, (1930), p1303.

14. Itoh, T. "Overview," *Ion Beam Asissted Film Growth*, edited by Tadatsugu Itoh. Elsevier Science Publishers B.V., 1989.

15. Yamamura, Y. and Noriaki Itoh. "Sputtering Yield," *Ion Beam Asissted Film Growth*, edited by Tadatsugu Itoh. Elsevier Science Publishers B.V., 1989.

16. Pulker, H. K. *Coatings on Glass.* Elsevier Science Publishers B.V., 1984.

17. Harper, J. M. E. and J. J. Cuomo. "Technology and Applications of Broad-Beam Ion Sources Used in Sputtering. Part II. Applications," *Journal of Vacuum Science Technology, 21*, (1988) p737.

18. Kuhman, D., S. Grammatica, and F. Jansen. "Properties of Hydrogenated Amorphous Silicon Carbide Films Prepared by Plasma-Enhanced Chemical Vapor Deposition," *Thin solid Films, 177*, (1989), p253.

19. Saito, N. "Effect of Hydrocarbon Gas on the Properties of Magnetron Sputtering of Amorphous SiC:H," *Journal of Non-Crystalline Solids, 108*, (1989), p211.

20. Le Contellec, M., J. Richard, and A. Guivarc'h. "Effects of the Silicon-to-Carbon Ratio and the Hydrogen Content in Amorphous SiC Thin Films Prepared by Reactive Sputtering," *Thin Solid Films, 58*, (1979), p407.

21. Smith, G. B. "Optical Properties of Chemically Ordered Silicon-Carbide Alloys," *Journal of Applied Physics, 65*, (1989), p1694.

22. Williamson, D. L., et al. "Microvoids in Amorphous $Si_{1-x}C_x$:H Alloys Studied by Small-Angle X-Ray Scattering," *Applied Physics Letters, 55*, (1989), p783.

23. Petrich, M. A. and J. A. Reimer. "Carbon Local Bonding Configurations in Amorphous Hydrogenated Silicon-Carbon Alloys," *Material Research Society Symposium Proceedings, 95*, (1987), p329.

24. Bhan, M. K., L. K. Malhotra, and S. C. Kashyap. "Infrared and Ellipsometric Studies of Reactive-Ion-Beam-Sputtered Amorphous Silicon (a-Si:H), Germanium (a-Ge:H) and Si-Ge Alloy (a-$Si_{28}Ge_{72}$:H) Films - A Correlation," *Thin Solid Films, 197*, (1991), p269.

25. Rizk, R. B., et al. "Sputtered Films of Amorphous Hydrogenated Silicon Carbide," *Material Research Society Symposium Proceedings, 97*, (1987), p295.

26. Saraie, J. "Preparation of Hydrogenated Amorphous Si-C Alloy Films and their Properties," *Thin Solid Films, 117*, (1984), p59.

27. Bhan, M. K., L. K. Malhotra, S. C Kashyap. "Electrical, Optical, and Structural Properties of Reactive Ion Beam Sputtered Hydrogenated Amorphous Germanium (a-Ge:H) Films," *Journal of Applied Physics, 65*,(1989), p241.

28. Bahn, M. K., L. K. Malhotra, S. C Kashyap. "Electrical and Optical Properties of Hydrogenated Amorphous Silicon-Germanium (a-$Si_{1-x}Ge_x$:H Films Prepared by Reactive Ion Beam Sputtering," *Journal of Applied Physics, 66*, (1989), p2528.

29. Sward, M. L. "Determination of the Optical Properties of Organic Thin Films by Spectroscopic Ellipsometry," AFIT GEP-90D-8, Master's Thesis, (Unpublished), (1990).

30. Lorraine, P. and Dale R. Corson. *Electromagnetic Fields and Waves.* W. H. Freeman and Company, 1970.

31. Azzam, R. M. A. and N. M. Bashara. *Ellipsometry and Polarized Light.* North-Holland, 1977.

32. Feldman, A. C. and J. W. Mayer. *Fundamentals of Surface and Thin Film Analysis.* North-Holland, 1986.